Doctoral Theses at NTNU, 2005:179

Eivind Smørgrav

Critical properties of effective gauge theories for novel quantum fluids

Doctoral Thesis

NTNU
Norwegian University of
Science and Technology
Doctoral thesis
for the degree of doktor ingeniør
Faculty of Natural Sciences and Technology
Department of Physics

NTNU
Innovation and Creativity

Abstract

Critical properties of $U(1)$ symmetric gauge theories are studied in 2+1 dimensions, analytically through duality transformations and numerically through Monte Carlo simulations. Physical applications range from quantum phase transitions in two dimensional insulating materials to superfluid and superconducting properties of light atoms such as hydrogen under extreme pressure. A novel finite size scaling method, utilizing the third moment M_3 of the action, is developed. Finite size scaling analysis of M_3 yields the ratio $(1+\alpha)/\nu$ and $1/\nu$ separately, so that critical exponents α and ν can be obtained independently without invoking hyperscaling. This thesis contains eight research papers and an introductory part covering some basic concepts and techniques.

Paper I [1]: The novel M_3 method is introduced and employed together with Monte Carlo simulations to study the compact Abelian Higgs model in the adjoint representation with $q = 2$. We find that α and ν vary along the critical line of the theory, and propose that it is a fixed line theory. The results are related to a recent microscopic description of zero temperature quantum phase transitions within insulating phases of strongly correlated systems in two spatial dimensions. We propose the above fixed line theory to be that of the *quantum phase transition* from a Mott-Hubbard insulator to a charge fractionalized insulator in two spatial dimensions.

Paper II [2]: We study phase transitions in the compact Abelian Higgs model for fundamental charge $q = 2, 3, 4, 5$. Various other models are studied to benchmark the M_3 method. For $q = 3$ we find a phase transition line which is first order below a *tricritical* point, and second order above. For all other integer $q \geq 2$ we have considered, the entire phase transition line is critical. The $q = 2$ results of **Paper I** are given in greater detail and at a higher level of accuracy.

Paper III [3]: This is a proceeding paper based on a talk given by F. S. Nogueira at the Aachen EPS HEP 2003 conference. A review of the results from **Paper I** and **Paper II** on the compact Abelian Higgs model together with some results on $q = 1$ obtained by F. S. Nogueira, H. Kleinert, and A. Sudbø is given.

Paper IV [4]: The effect of a Chern-Simons (CS) term in the phase structure of two Abelian gauge theories is studied. For the compact Maxwell-Chern-Simons theory we obtain that for values $g = n/2\pi$ of the CS coupling with $n = \pm 1, \pm 2, \ldots$ the theory is equivalent to a gas of closed loops with contact interaction, exhibiting a phase transition in the 3D XY universality class. We also employ Monte Carlo simulations in combination with M_3 analysis to study the non-compact $U(1)$ Abelian Higgs model with a CS term. The critical exponents α and ν vary continuously with the strength of the CS term.

Paper V [5]: We study the critical properties of the N-component Ginzburg-Landau theory. The model is dualized to a theory of N vortex fields interacting through a Coulomb and a screened potential. The model with $N = 2$ components exhibits two anomalies in the specific heat. From the critical exponents α and ν, the mass of the gauge field, and the vortex correlation functions, we conclude that one anomaly corresponds to a charged *inverted* 3D XY fixed point, while the other corresponds to a neutral 3D XY fixed point. For arbitrary N there are N fixed points, one corresponding to an inverted 3D XY fixed point and $N-1$ corresponding to neutral 3D XY fixed points.

Paper VI [6]: We consider the vortices in the 2-component Ginzburg-Landau model in a finite but low magnetic field. The ground state is a lattice of co centered vortices in both order parameters. We find two novel phase transitions. *i*) A "vortex sub-lattice melting" transition where vortices in the field with lowest phase stiffness ("light vortices") loose co centricity with the vortices with large phase stiffness ("heavy vortices"), entering a liquid state. Remarkably, the structure factor of the light vortices vanishes *continuously* and this transition is in the 3D XY universality class. *ii*) A first order melting transition of the lattice of heavy vortices *in a liquid of light vortices*.

Paper VII [7]: The phase diagram and critical properties of the N-component London superconductor are studied in zero and finite magnetic field. Direct and dual gauge field correlators for general N are given. The model with $N = 3$ exhibits three anomalies in the specific heat. We demonstrate the existence of two neutral 3D XY fixed points and one inverted charged 3D XY fixed point. For the general case, we explicitly identify one charged vortex mode and $N-1$ neutral vortex modes. The model for $N = 2$ and equal bare phase stiffnesses corresponds to a field theoretical description of an easy plane quantum antiferromagnet. In this case, the critical exponents are computed and found to be different from 3D XY values. The N-component model in an external magnetic field, is shown to have a novel feature of $N - 1$ superfluid phases arising out of N charged condensates. In particular, for $N = 2$ we point out the possibility of two novel types of field induced phase transitions in ordered quantum fluids: *i)* A phase transition from a superconductor to a superfluid or vice versa, driven by tuning an external magnetic field. *This identifies the superconducting phase of liquid metallic hydrogen as a novel quantum fluid. ii)* A phase transition corresponding to a quantum fluid analogue of sub-lattice melting, where a composite field induced Abrikosov vortex lattice is decomposed and disorders the phases of the constituent condensate with lowest bare phase stiffness. Both transitions belong to the 3D XY universality class. For $N \geq 3$, there is a new feature not present in the cases $N = 1$ and $N = 2$, namely a partial decomposition of composite field induced vortices driven by thermal fluctuations.

Paper VIII [8]: We study the phase structure of a 2-component superconductor in a high magnetic field. We identify a regime where first, at a certain temperature a field induced lattice of co centered vortices of both order parameters melts, causing the system to loose superconductivity. In this state the system retains a broken composite symmetry and we observe that at a higher temperature T_c it undergoes another phase transition where the disordered composite vortex lines are "ionized" into a "plasma" of constituent vortex lines in individual order parameters. This is the hallmark of the superconductor-to-superfluid-to-normal fluid phase transitions projected to occur in e.g. liquid metallic hydrogen.

Acknowledgment

First I want to express my deepest gratitude to Professor *Asle Sudbø* for giving me the opportunity to be his doctorate student. Asle is extremely dedicated and passionate when it comes to physics, and I have been very fortunate to work on problems to which Asle has been dedicated. This has given me almost unlimited access to his time, and I am indebted for everything that he has taught me and for promoting my research. I am confident that I could not possibly have received better guidance.

During my entire Ph.D. period I have been rooming and collaborating closely with *Jo Smiseth*. This has been a true pleasure. I strongly believe that we have accomplished far more together than twice the amount that I could have managed on my own. I have really appreciated his company these years, and I am happy that I will continue cooperating with him in the future.

Figure 1: Our group as it appeared August 26th. 2005. From the left: Egor Babaev, Eivind Smørgrav, Kjetil Børkje, Lars Erik Walle, Martin Grønsleth, Jo Smiseth, Asle Sudbø, Eskil Kulseth Dahl, Steinar Kragset, and Joakim Hove.

Next I want to acknowledge a number of people that have contributed to this thesis in various ways. *Egor Babaev* is acknowledged for introducing me to the exciting field of liquid metallic hydrogen and the multi component Ginzburg-Landau theories. Egor has also been entertaining me late evenings at the office by sharing his opinions on everything from anthropology to second hand cars. *Joakim Hove* gave me the softest possible transition to my scientific career, by generously donating his computer code and patiently introducing me to everything from parallel computing to vortex physics. *Flavio Nogueira* is acknowledged for close collaboration on the first four articles. *Kari Rummukainen* is acknowledged for generously letting me use his Ferrenberg-Swendsen reweighting software, without which most of this work would have been impossible.

Neil Ashcroft has had an indirect, but important influence on the last four articles through Egor, and he generously met with Jo and me at the 2005 APS March meeting. *Vilde Tingleff*, *Øyvind Tingleff*, *Kjetil Børkje*, and *Steinar Kragset* are acknowledged for helping me with this manuscript. Finally a warm thanks goes to all coffee drinkers and lunch eaters for a jolly good time. I am indebted to each and every one of you.

The Department of Physics at NTNU is gratefully acknowledged for financing this work through a university fellowship. Moreover, I thank The Research Council of Norway and NTNU for funding a huge amount of computation time, roughly 1200 000 CPU-hours in total, on the SGI Origin 3800 parallel computers.

I also want to thank *Zlatko Tešanović*, *Ernst Helmut Brandt*, and *Kristian Fossheim* for agreeing to participate on the evaluation committee of this thesis.

Last, but not least, I will thank my family *Vetle*, *Hanne*, and *Hege* for loving me and putting up with long hours at work.

Trondheim, September 2005

Eivind Smørgrav

List of Publications

Paper I: A. Sudbø, E. Smørgrav, J. Smiseth, F.S. Nogueira, and J. Hove, *Criticality in the (2 + 1)-Dimensional Compact Higgs Model and Fractionalized Insulators*,
Physical Review Letters **89**, 226403 (2002).

Paper II: J. Smiseth, E. Smørgrav, F.S. Nogueira, J. Hove, and A. Sudbø, *Phase structure of (2+1)-dimensional compact lattice gauge theories and the transition from Mott insulator to fractionalized insulator*,
Physical Review B **67**, 205104 (2003).

Paper III: F.S. Nogueira, J. Smiseth, E. Smørgrav, and A. Sudbø, *Compact U(1) gauge theories in 2+1 dimensions and the physics of low dimensional insulating materials*,
European Physical Journal C **33**, 885 (2004).

Paper IV: E. Smørgrav, J. Smiseth, A. Sudbø, and F.S. Nogueira, *Phase structure of Abelian Chern-Simons gauge theories*,
Europhysics Letters **68**, 198 (2004).

Paper V: J. Smiseth, E. Smørgrav, and A. Sudbø, *Critical Properties of the N-Color London Model*,
Physical Review Letters **93**, 077002 (2004).

Paper VI: E. Smørgrav, J. Smiseth, E. Babaev, and A. Sudbø, *Vortex Sublattice Melting in a Two-Component Superconductor*,
Physical Review Letters **94**, 096401 (2005).

Paper VII: J. Smiseth, E. Smørgrav, E. Babaev, and A. Sudbø, *Field- and temperature-induced topological phase transitions in the three-dimensional N-component London superconductor*,
Physical Review B **71**, 214509 (2005).

Paper VIII: E. Smørgrav, E. Babaev, J. Smiseth, and A. Sudbø, *Observation of a Metallic Superfluid in a Numerical Experiment*,
Physical Review Letters **95**, 135301 (2005).

Contents

1 Introduction

Physics is about describing and explaining nature in terms of mathematics. Successful physical theories have in common the ability to pinpoint the important features of the problem and ignore the unimportant details. Usually, there is a whole hierarchy of different theories offered at different levels, describing the same phenomenon. For some purposes it suffices to treat a system classically, and for others a more microscopic approach, such as a quantum mechanical description, is appropriate. In this context effective theories have had an enormous success. The most notable example in solid state physics is perhaps the Fermi liquid theory of metals. The ingenious assumption that the electrons in an ordinary metal such as aluminum can essentially be approximated by a renormalized noninteracting electron gas with quantum numbers in one-to-one correspondence with the true noninteracting system, has given a tremendous insight in the physics of metals. The Fermi liquid theory is the corner stone in solid state physics, and it is hard to see how the alternative, *ab initio* calculations on all different metals, could have achieved the same success. Another notable example is the Landau-Ginzburg-Wilson theory approach to phase transitions and critical phenomena. This motivates the use of effective models in physics, even in the cases where there is no direct microscopic foundation, but where the theory is written down purely on symmetry grounds.

Some of the most fascinating phenomena in physics today are associated with strongly correlated systems in which collective quantum effects play a dominating role, leading to a breakdown of the Fermi liquid theory. Prominent examples of this are high temperature superconductivity and the quantum Hall systems. A main thrust of modern condensed matter physics is to characterize and explain these exotic phenomena. Typically, a solid state system consists of 10^{23} particles that interact in some fashion, thus an excellent framework to describe these strongly interacting degrees of freedom is field or gauge theory. Traditionally, gauge theories have been the domain of high energy physics, but with the discovery of the high temperature superconductors and the quantum Hall materials in the 1980s, it has become an important tool in solid state physics. The gauge theories of condensed matter physics basically come in two categories; the phenomenological theories written down on symmetry grounds such as the Ginzburg-Landau (GL) theory of superconductivity, and the emergent gauge theories deduced from some underlying microscopic model. In the former case the gauge field is typically the electromagnetic vector potential that couples minimally through the charge of a particle, whereas in the latter case the gauge field is typically some emergent field enforcing a local constraint.

This thesis is about critical properties of various $U(1)$ gauge theories in 3 or (2+1) dimensions. We have studied the compact Abelian Higgs model in **Paper I** [1], **Paper II** [2], and **Paper III** [3]. For fundamental coupling $q = 2$ this is an effective theory for two types of bosons hopping on a two dimensional lattice. In **Paper IV** [4] we studied

the effect of a Chern-Simons term on the critical properties of two different $U(1)$ gauge theories. In **Paper V** [5] and **Paper VII** [7] we studied the 2-component GL model and its N-component generalization in zero magnetic field. Finally in **Paper VI** [6] and **Paper VIII** [8] we studied the 2-component GL model in an external magnetic field.

The $N = 2$ GL model can be thought of as a phenomenological model of a superconductor with two individually conserved matter fields. One candidate system with these properties is liquid metallic hydrogen, projected to become superconducting with both electronic and protonic Cooper pairs at extreme pressure [9, 10]. An ordinary superconductor may set up a dissipationless supercurrent of charges when it is subjected to a DC current or a magnetic field. A superfluid, like ^{4}He, is able to set up a dissipationless flow of mass in a rotating container. We show that the 2-component GL model possesses two modes, one neutral mode resembling the theory of a superfluid and one charged mode resembling the theory of a superconductor. The physical consequence of this is that the system is able to sustain both dissipationless *co directed* and *counter directed* flows of superconducting electrons and protons protected by the neutral and charged modes, respectively. When this system is exposed to an external magnetic field, it can sustain four different phases. At low temperature and low magnetic field it may sustain both superfluidity and superconductivity. This means that if the system is subjected to a DC current or a magnetic field it may set up a *counter directed* flow of electrons and protons. On the other hand, if the system is rotated it will set up a *co directed* supercurrent of electrons and protons, where there is no net transport of charge but dissipationless transport of mass. Thus, this system cannot be characterized exclusively as a superfluid or as a superconductor; it is a novel quantum fluid combining the two properties. Another phase at high magnetic field and intermediate temperature sustains superfluidity in a metallic background. Thus if the state of liquid metallic hydrogen is ever realized, it should display two novel quantum fluids; the superfluid superconductor and the metallic superfluid.

The same model describing the liquid metallic hydrogen, but with equal phase stiffnesses for the two condensates, is suggested as an effective model for an easy plane quantum antiferromagnet in two dimensions at zero temperature [11–14]. In this case the matter fields originate with a bosonic representation of spin operators, and the theory is claimed to describe a transition from a Neél state to a paramagnetic valence bond ordered state.

The surprising fact that two such apparently disparate physical systems can be described by the same theory displays the strength and beauty of gauge theories. Critical properties and phase structure of physical systems are largely independent of microscopic details, but rely on a few important aspects such as symmetries and dimensionality. Thus, in writing down the field theory of a system one is forced to sort out these questions. Once this is done, the field theory provides a clean model to study these matters analytically or numerically on a computer.

The outline of this thesis is as follows. First I give a brief introduction to some models, concepts, and techniques necessary to understand the papers listed above. Chapter 2 covers phase transitions, Chapter 3 covers topological excitations and duality, and Chapter 4 covers Monte Carlo techniques including some post processing techniques. In Chapter 5, I give a tour of the results obtained on the $N = 2$ GL model and its application to liquid metallic hydrogen. In my opinion, this is the most exotic and least known of the physical systems we have investigated. Thus it should be of interest to most readers, and yet it captures the essential physics needed to understand the topics

of the other papers.

2 Phase Transitions

Matter appear in many different states such as solids, liquids, and vapors, metals can become ferromagnetic or antiferromagnetic and some even become superconducting. A main thrust of condensed matter physics is to identify, characterize, and explain the different states of matter and the transitions between them. Some of these transitions, like the boiling and freezing of water, are every day phenomena vital to life as we know it. The modern investigation of phase transitions can be said to start in 1869 with the discovery of Thomas Andrews that there is a special point for CO_2 at about 31°C and 73 atmospheres pressure where the liquid phase and the vapor become indistinguishable [15]. Curiously enough, CO_2 becomes opaque in the vicinity of this point. Thirty years later Pierre Curie discovered that iron also displays a special point which is the highest temperature in zero magnetic field where iron can remain permanently magnetized [16]. Curie realized the parallel between the density-temperature curves of CO_2 and his magnetization-temperature curve for iron, and denoted such points critical points.

The theory of phase transitions can roughly be divided into two types of problems; what are the interactions responsible for a particular transition, and how should one characterize and handle a transition once the governing forces are known. In this chapter I will mainly deal with the latter question. First I will introduce some necessary notation from statistical mechanics, then I will introduce some models, and finally go through some important concepts that are used throughout this thesis. The general references that I have used for this chapter are [17–23].

2.1 Statistical Mechanics

The difficulty associated with phase transitions is that they occur in ensembles of many, say 10^{23}, particles. Instead of solving the equations of motion for all these particles, statistical mechanics attempts to treat them in a probabilistic way by considering macroscopic quantities such as pressure, magnetization, and density. The central quantity is the Hamiltonian H, which gives the total energy of the system in a given state. In thermal equilibrium with a reservoir at temperature T the microscopic states $\{\Psi\}$ are distributed according to the Boltzmann probability

$$p_{\mathrm{B}} = \frac{1}{\mathcal{Z}} e^{-\beta H[\Psi]}, \tag{2.1}$$

where $\beta = 1/k_{\rm B}T$ is inverse temperature and $k_{\rm B}$ is the Boltzmann constant. The normalization constant $\mathcal{Z}$ is the partition function defined by

$$\mathcal{Z} = \int \mathcal{D}\Psi e^{-\beta H[\Psi]}, \tag{2.2}$$

which is a functional integral over all states Ψ of the system. All possible physics of a system is encoded in the partition function, and thermodynamic quantities such as the internal energy $U = -\partial \ln \mathcal{Z}/\partial\beta$, the specific heat $C_V = -k_{\rm B}\beta^2\partial^2 \ln \mathcal{Z}/\partial\beta^2$, and the Helmholtz free energy $F = -\frac{1}{\beta}\ln \mathcal{Z}$,

$$F = U - TS, \tag{2.3}$$

are directly related to it. Thus, the problem of understanding phase transitions can be reduced to calculating the partition function for various Hamiltonians.

At the simplest level, phase transitions can be understood from Eq. (2.3) in the following way; a phase is stable if the free energy F has a minimum and is a smooth analytic function for the particular temperature regime. Minimizing F can be done in one of two ways. At low temperature it is done by lowering the internal energy U, which means ordering the system. At higher temperatures F is minimized by increasing the entropy S, which is done by disorganizing the system. However, achieving both low U and high S are conflicting goals, and phase transitions may emerge from the competition between the two. The low temperature phase will be denoted the ordered state and the high temperature phase will be denoted the disordered phase.

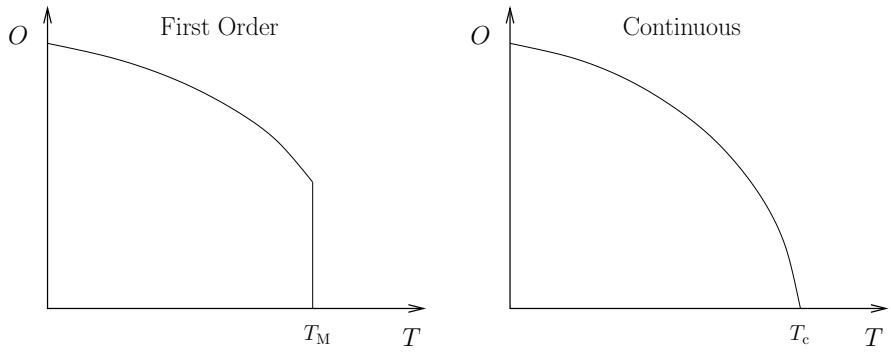

Figure 2.1: The order parameter O plotted against temperature for a first order (left panel) and a continuous phase transition (right panel).

The system abruptly changes its macroscopic behavior when temperature is tuned through a phase transition. Whereas stable phases have analytic and smooth thermodynamic variables, phase transitions are associated with singularities and non-analytic behavior in these variables. There are basically two ways that such a transition can occur. The first possibility is that the two different phases coexist at the phase boundary. Since the distinct phases have different macroscopic properties, these must be discontinuous at the phase transition. Such transitions are denoted discontinuous or first order phase transitions, and are associated with a latent heat which is released as the system

passes through the transition from below. The other possibility is the continuous or second order phase transitions where the two phases become alike at the phase boundary. These transitions are characterized by a diverging correlation length ζ, which means that fluctuations are correlated at all length scales. This forces the system to be in one unique critical phase and the differences in macroscopic variables on both sides of the transition go smoothly to zero.

2.2 Spontaneous Symmetry Breaking

Let $\mathcal{G}$ be the symmetry group containing all the symmetry operations under which the Hamiltonian H is invariant. This means that if G is a representation of $\mathcal{G}$ and

$$H(G\Psi) = H(\Psi), \tag{2.4}$$

H possesses the symmetries of $\mathcal{G}$. In general the high temperature disordered phase is invariant under the same symmetry group as the Hamiltonian. All observables that are affected by operations in $\mathcal{G}$ have zero thermal averages. Ordered phases are distinguished from disordered phases by the appearance of thermodynamic averages of observables O which are not invariant under $\mathcal{G}$. This means that the symmetry group of the ordered state $\mathcal{G}_o$ is smaller than $\mathcal{G}$, and the symmetry $\Delta\mathcal{G} = \mathcal{G} - \mathcal{G}_o$ is said to spontaneously broken. The observables O are called order parameters, see Fig. 2.1.

2.2.1 Ising Model

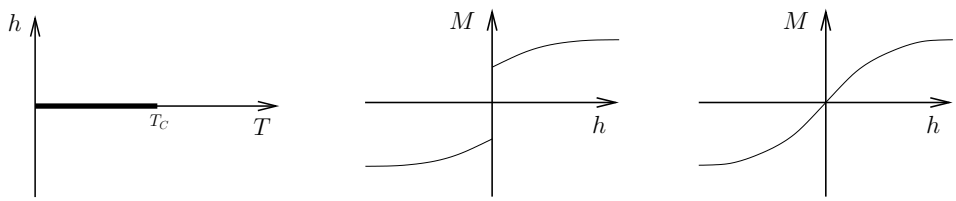

Figure 2.2: Left panel: the phase diagram of the 2D Ising model. Middle panel: the magnetization $M(h)$ for a fixed temperature below T_c experiences a discontinuity at $h = 0$, corresponding to a first order phase transition. Right panel: the magnetization $M(h)$ for a fixed temperature above T_c is continuous across $h = 0$.

The Ising model is a microscopic model for an easy axis ferromagnet, where spins can point either up or down on a regular lattice. The spins interact with their nearest neighbors so that it is energetically favorable to point in the same direction. The Hamiltonian is given by

$$H = -J \sum_{\langle i,j \rangle} S_i S_j - h \sum_i S_i, \tag{2.5}$$

where $S_i \in \{1, -1\}$ is the spin at site i, $\langle i, j \rangle$ means sum over nearest neighbors, $J > 0$ is the ferromagnetic coupling constant, and h is a magnetic field parallel to the axis of the magnet. The Ising model is a sort of minimal model in the theory of phase transitions,

in the sense that it captures the essential physics of the phenomenon. Lars Onsager solved this model analytically in $d = 2$ dimensions for $h = 0$ through a *tour de force* in 1944 [24].

The magnetization

$$M = \frac{1}{N} \left\langle \sum_i S_i \right\rangle, \tag{2.6}$$

where N is the total number of spins and $\langle\ \rangle$ means thermal average, is a good order parameter for this system. The $h - T$ phase diagram is shown in the left panel of Fig. 2.2. Above the line $h = 0$ spins collectively align up and below $h = 0$ they align down. The line $h = 0$ for $T < T_c$ corresponds to a first order phase transition, where the magnetization is discontinuous when h is varied across this line. The line $h = 0$ for $T > T_c$ is not associated with any singularities and the magnetization is continuous when crossing this line. At $T = T_c$ however, the first order line ends at a critical point, i.e. a second order phase transition. For $h = 0$ the Hamiltonian Eq. (2.5) is invariant with respect to flipping all spins

$$S_i \to -S_i \quad \forall\ i \in [1, \ldots, N]. \tag{2.7}$$

This is a global Z_2 or Ising symmetry. In the disordered phase the magnetization is invariant under the Z_2 symmetry, but when temperature is lowered across T_c the spins spontaneously align in some arbitrary direction, the Z_2 symmetry is broken, and M attains an expectation value.

2.2.2 XY Model

The XY model describes an easy plane ferromagnet where spins are free to rotate in the xy plane

$$H = -J \sum_{\langle i,j \rangle} \mathbf{S}_i \cdot \mathbf{S}_j = -J \sum_{\langle i,j \rangle} \cos\left(\theta_i - \theta_j\right), \tag{2.8}$$

where $\mathbf{S}_i$ is a two-component vector with length $|\mathbf{S}_i| = 1$. Alternatively, superfluid helium may be described by this model, through a macroscopic condensate wave function $\psi(\mathbf{r}) = |\psi| e^{\mathrm{i}\theta_i}$. The Hamiltonian Eq. (2.8) is invariant with respect to rotating all spins an angle φ

$$\theta_i \to \theta_i + \varphi \quad \forall\ i \in [1, \ldots, N]. \tag{2.9}$$

This is a global $U(1)$ symmetry. The Mermin-Wagner theorem states that a continuous symmetry cannot be spontaneously broken in a system with dimensionality less than or equal to 2 [25]. Nevertheless, the 2D XY model exhibits the famous Berezinskii-Kosterlitz-Thouless transition [26,27], in which the low temperature ordered phase with power law correlation functions evolves into the disordered phase which exhibits exponentially decaying correlation functions. In $d = 3$ dimensions the XY model goes through a second order phase transition in which the spins spontaneously align in an arbitrary direction to spontaneously break the $U(1)$ symmetry. A global order parameter for this transition is the helicity modulus Υ [28–30], which probes the stiffness with respect to a twist in the phase. Formally it is defined as the second derivative of the free energy with respect to a twist $\delta\theta$,

$$\Upsilon = \frac{1}{3N} \left\langle \sum_{i\mu} \cos\left(\Delta_\mu \theta_i\right) \right\rangle - \frac{J\beta}{3N} \left\langle \left[\sum_{i,\mu} \sin\left(\Delta_\mu \theta\right) \right]^2 \right\rangle, \tag{2.10}$$

where Δ_μ is the lattice differential operator. In the case of superfluidity, Υ may be viewed as the superfluid density. When $\Upsilon > 0$ there is global phase coherence and when $\Upsilon = 0$ this coherence is lost, thus Υ probes the superfluid to normal phase transition in helium.

2.2.3 Ginzburg-Landau Model

The Ginzburg-Landau (GL) model was originally written down based on symmetry and physical intuition by Vitaly Ginzburg and Lev Landau in 1950 [31]. The theory describes a charged condensate, i.e. a superconductor, through a local complex matter field $\Psi(\mathbf{r})$ which couples minimally to the electromagnetic gauge field $\mathbf{A}(\mathbf{r})$,

$$H = \int \mathrm{d}\mathbf{r} \left[\alpha(\tau)|\Psi(\mathbf{r})|^2 + \frac{u}{2}|\Psi(\mathbf{r})|^4 + \frac{1}{2m}|(\nabla - \mathrm{i}e\mathbf{A}(\mathbf{r}))\Psi(\mathbf{r})|^2 + \frac{1}{2}(\nabla \times \mathbf{A}(\mathbf{r}))^2 \right], \tag{2.11}$$

where $\alpha(\tau) = \alpha_0(T - T_{\mathrm{MF}})$ is the temperature dependent coupling constant that drives the system through the phase transition, T_{MF} is the mean field transition temperature, e and m are the effective charge and mass of a Cooper pair, and u is a temperature independent GL parameter[1]. The amplitude $|\Psi(\mathbf{r})|^2$ is to be interpreted as the local density of Cooper pairs. The model can be shown to have two length scales

$$\lambda(\tau) = \sqrt{\frac{mu}{4e^2\alpha(\tau)}}, \qquad \xi(\tau) = \sqrt{\frac{1}{2m\alpha(\tau)}}, \tag{2.12}$$

where λ is the magnetic penetration length which sets the scale for the screening of a magnetic field and ξ is the correlation length which sets the scale over which $|\Psi(\mathbf{r})|$ varies. The Ginzburg-Landau parameter $\kappa = \lambda/\xi$ is a dimensionless parameter in the problem.

The Ginzburg-Landau Hamiltonian Eq. (2.11) is invariant with respect to a local $U(1)$ symmetry ($U(1)$ gauge symmetry)

$$\Psi(\mathbf{r}) \to \Psi(\mathbf{r})e^{\mathrm{i}\varphi(\mathbf{r})} \qquad \mathbf{A}(\mathbf{r}) \to \mathbf{A}(\mathbf{r}) + \frac{1}{e}\nabla\varphi(\mathbf{r}). \tag{2.13}$$

This means that the symmetry operation may be performed in a local region in space, involving a finite number of variables. Elitzur's theorem states that a local symmetry cannot be spontaneously broken, since non gauge invariant quantities are bound to zero by symmetry [32]. Consequently, a phase transition in a system with local symmetry cannot have a *local order parameter*. For $\kappa > \kappa_{\mathrm{tri}}$ the Ginzburg-Landau model Eq. (2.11) exhibits a second order phase transition in which the gauge field $\mathbf{A}$ attains a mass $m_{\mathbf{A}}$ through the Anderson-Higgs phenomenon [33, 34]. For $\kappa < \kappa_{\mathrm{tri}}$, the phase transition is first order [35]. In reference [35], it was furthermore established that the difference between type I and type II behavior is the same as the difference between superconductors exhibiting first and second order phase transitions. The mean field value of $\kappa_{\mathrm{tri}} = 1/\sqrt{2}$. Through large scale MC simulations, the tri-critical value of κ has been determined to be $\kappa_{\mathrm{tri}} = (0.76 \pm 0.04)/\sqrt{2}$ [35].

[1] Note that c, $\hbar$, and μ_0 have been put to one for notational convenience.

2.2.4 London Model

For strong type II superconductors, i.e. large κ, the fluctuations in the amplitude $|\Psi(\mathbf{r})|$ can be neglected and the matter field takes on the form $\Psi(\mathbf{r}) = |\Psi|e^{i\theta(\mathbf{r})}$. This is the London approximation which leads to the London superconductor model

$$H = \int \mathrm{d}\mathbf{r} \left[\frac{|\Psi|^2}{2m} (\nabla\theta(\mathbf{r}) - e\mathbf{A}(\mathbf{r}))^2 + \frac{1}{2}(\nabla \times \mathbf{A}(\mathbf{r}))^2 \right]. \tag{2.14}$$

This Hamiltonian exhibits the local $U(1)$ symmetry

$$\theta(\mathbf{r}) \to \theta(\mathbf{r}) + \varphi(\mathbf{r}) \qquad \mathbf{A}(\mathbf{r}) \to \mathbf{A}(\mathbf{r}) + \frac{1}{e}\nabla\varphi(\mathbf{r}). \tag{2.15}$$

In $d = 3$ dimensions the London model Eq. (2.14) always undergoes a second order phase transition in which the gauge field $\mathbf{A}$ attains a mass $m_{\mathbf{A}}$.

The mass of the gauge field $m_{\mathbf{A}}$ is a global quantity that may be extracted from correlators. The local magnetic field $\mathbf{B}(\mathbf{r}) = (\nabla \times \mathbf{A}(\mathbf{r}))$ is a gauge invariant operator which can attain a nonzero expectation value. Its correlator is defined by

$$G_{\mathbf{B}}(\mathbf{r}) = \langle \mathbf{B}(0) \cdot \mathbf{B}(\mathbf{r}) \rangle \,, \tag{2.16}$$

and the Fourier transform is defined by

$$\mathcal{G}_{\mathbf{B}}(\mathbf{q}) = \langle \mathbf{B}(-\mathbf{q}) \cdot \mathbf{B}(\mathbf{q}) \rangle \,. \tag{2.17}$$

The general structure of $\mathcal{G}_{\mathbf{B}}(\mathbf{q})$ is

$$\mathcal{G}_{\mathbf{B}}(\mathbf{q}) \sim \frac{2\mathbf{q}^2/\beta}{\mathbf{q}^2 + \Sigma(\mathbf{q})}, \tag{2.18}$$

where $\Sigma(\mathbf{q})$ is the self energy of the system. Close to the critical point this can be fitted to the Ansatz [36]

$$\Sigma(\mathbf{q}) = m_{\mathbf{A}}^2 + A|\mathbf{q}|^{2-\eta} + \mathcal{O}(|\mathbf{q}|^{\delta}), \tag{2.19}$$

where η is a critical exponent which is to be discussed later. Thus $m_{\mathbf{A}}$ can be obtained from

$$m_{\mathbf{A}}^2 = \lim_{\mathbf{q}\to 0} \frac{2\mathbf{q}^2}{\beta} \mathcal{G}_{\mathbf{B}}^{-1}(\mathbf{q}). \tag{2.20}$$

Since $\mathcal{G}_{\mathbf{B}}(\mathbf{q})$ is the correlator of the magnetic field, $m_{\mathbf{A}}$ may be identified as the inverse of the magnetic penetration length λ. Thus the Higgs mechanism is in fact synonymous with the Meissner effect in this case. In Chapter 3 it will be shown how to relate $m_{\mathbf{A}}$ to vortex correlators.

2.3 Critical Exponents

The critical behavior of systems near a second order phase transition turns out to be insensitive to microscopic details, and the different models fall into a handful of different classes. These universality classes are characterized by global features such as the symmetries of the order parameter and the dimensionality of the system. The diverging

Table 2.1: Definitions of the Critical Exponents.

Definition						
C_V	$\propto$	$\partial^2 F/\partial T^2$	$\sim$	$\lvert T-T_c\rvert^{-\alpha}$	$T \to T_c^{\pm}$	$h=0$
χ	$\propto$	$\partial^2 F/\partial h^2$	$\sim$	$\lvert T-T_c\rvert^{-\gamma}$	$T \to T_c^{\pm}$	$h=0$
M	$\propto$	$\partial F/\partial T$	$\sim$	$\lvert T-T_c\rvert^{\beta}$	$T \to T_c^{-}$	$h=0$
M	$\propto$	$\partial F/\partial T$	$\sim$	$\lvert h\rvert^{1/\delta}$	$T=T_c$	$h \to 0^{\pm}$
Γ	$\propto$	$\langle S(0)S(r)\rangle - \langle S\rangle^2$	$\sim$	$r^{-(d-2+\eta)}$	$T=T_c$	$h=0$
ζ	$\propto$	$e^{-r/\zeta}$	$\sim$	$\lvert T-T_c\rvert^{-\nu}$	$T \to T_c^{\pm}$	$h=0$

correlation length ζ and other thermodynamic properties exhibit power law dependencies with respect to their distance from the critical point. These powers are denoted critical exponents, and the complete set of these determines the universality class of the system.

In the language of the Ising model, the behavior of the specific heat C_V as the critical point is approached along the line $h = 0$ is governed by the critical exponent α,

$$C_V \sim |T - T_c|^{-\alpha}. \tag{2.21}$$

For most models $\alpha > 0$ and C_V diverges at the transition, but typically α is small and the divergence is slow. For the 3D XY model for instance, α is negative, which means that C_V is finite across the phase transition. Thus a better scaling Ansatz [18] for the specific heat would be

$$C_V \sim \frac{1}{\alpha}\left(|T - T_c|^{-\alpha} - 1\right). \tag{2.22}$$

Away from the phase transition and for large distances r the spin-spin correlation function behaves like

$$\Gamma(r) \equiv \langle S(0)S(r)\rangle - \langle S(0)\rangle^2 \sim \exp\left(r/\zeta\right). \tag{2.23}$$

At the critical point however, the correlation length ζ diverges with critical exponent ν

$$\zeta \sim |T - T_c|^{-\nu}, \tag{2.24}$$

and the correlation function itself goes as a power law determined by the anomalous dimension η

$$\Gamma(r) \sim r^{-(2-d-\eta)}. \tag{2.25}$$

Altogether there are six critical exponents, and these are summarized in Table 2.1.

The exponents α, β, γ, δ, ν and η are in fact not independent of each other. There are four relations between them. This should really be shown within the framework of the renormalization group, but I will refer the reader to the general literature on this [17, 18], and use the homogeneity postulate of Widom [37],

$$F_s(|\tau|, h) \sim b^{-d} F_s(|\tau| b^{1/\nu}, h b^{\lambda_h}), \tag{2.26}$$

assumed to be valid in the vicinity of the critical point. Here F_s is the singular part of the Helmholtz free energy Eq. (2.3), $\tau = T - T_c$, b is some arbitrary scaling factor, and λ_h yet another constant. By differentiating Eq. (2.26) in various ways and equating the

results with the proper definitions from Table 2.1, the following relations emerge

$$\alpha + 2\beta + \gamma = 2 \tag{2.27}$$
$$\alpha + \beta(\delta + 1) = 2 \tag{2.28}$$
$$(2 - \eta)\nu = \gamma \tag{2.29}$$
$$2 - \alpha = d\nu. \tag{2.30}$$

Eq. (2.30) is called the hyperscaling relation and it couples the behavior of C_V with the behavior of the correlation function. The hyperscaling relation is known to be violated above the critical dimension $d_c = 4$ and in some systems in the presence of dangerously irrelevant operators. In these cases the operators influence the scaling of the free energy but not the correlation function [17].

2.4 Quantum Phase Transitions

Quantum critical phenomena are phase transitions in a quantum mechanical system that are driven by tuning a parameter in the Hamiltonian. Typically this parameter determines the strength between two non-commutative parts of the Hamiltonian. Within the formulation of functional integrals [38] the partition function of such a system is given by

$$\begin{aligned} \mathcal{Z} &= \int \mathcal{D}\Psi e^{-S} \\ S &= \frac{1}{\hbar} \int_0^\beta \mathrm{d}\tau \int \mathrm{d}^d\mathbf{r}\mathcal{L}, \end{aligned} \tag{2.31}$$

where S is the action of the system which is to be integrated over the d spatial dimensions and the imaginary time dimension τ. At $T = 0$ the imaginary time dimension takes on the form of an Euclidean dimension, and the above partition function Eq. (2.31) exactly resembles the classical partition function Eq. (2.2) in $D = d + 1$ dimensions where a coupling constant plays the role of the classical temperature. Thus a quantum mechanical problem at $T = 0$ may be mapped onto a classical problem in one higher dimension [39]. In **Paper I** [1] and **Paper II** [2] we study classical models in 3 dimensions as effective models for two-dimensional quantum mechanical problems.

3 Topological Objects and Duality

The origin of the strong fluctuations that are responsible for the destruction of order and the phase transitions described in the previous chapter is topological defects. In this chapter I will show that these objects play a key role in understanding the nature of these phase transitions. First I will introduce the concept of topological objects, and then show how the proliferation of these governs the various transitions. Next I will present the concept of duality and duality transformations. Finally, I will demonstrate in detail how the London model can be transformed into a theory of interacting vortex loops in the grand canonical ensemble. The details of the same transformation applied to the N-component London model are found in Appendix B of **Paper VII** [7]. The general references used in this chapter are [20, 40–49].

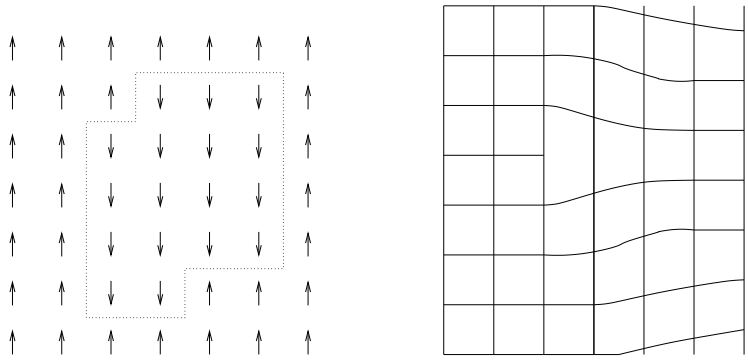

Figure 3.1: The left figure shows the topological defect of the 2D Ising model which is a domain line separating spins of different orientation. The figure to the right illustrates a lattice dislocation.

3.1 Topological Excitations

Topological defects are configurations that are able to destroy order at long distances at a fairly low cost of energy. The nature of the defects are non-local and therefore dependent of macroscopic properties such as dimensionality and symmetries. In general they can be characterized by some core region where order is destroyed, surrounded by

a large region in which the field varies smoothly in space. Since the defect only can be removed by varying a large number of variables around the center of the object, it is said to be topologically stable. Although there is an energy cost associated with creating the object, the configurational entropy will eventually exceed this when the temperature is increased. This leads to a permanent destruction of the order through a phase transition.

Topological defects have different names depending on the particular system in which they appear and the symmetry they break. In Ising models the defects are domain lines in $d = 2$ separating regions of oppositely aligned spins, as shown in Fig. 3.1, and domain walls in $d = 3$. In periodic solids they are called dislocations and are responsible for a wide range of mechanical properties of metals. In $U(1)$ theories the topological excitations are denoted vortices and vortex lines in two and three dimensions, respectively.

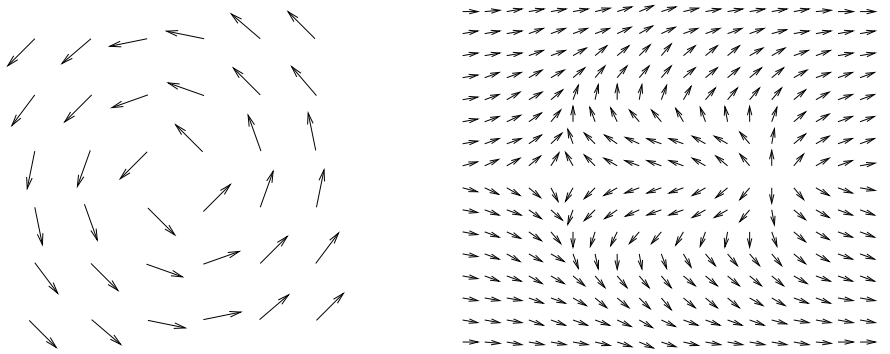

Figure 3.2: Left panel: one possible spin configuration of a vortex in the 2D XY model. Right panel: the spin configuration of a vortex pair in the 2D XY model.

The phase θ of the spin variables in a $U(1)$ theory changes continuously by an integer times 2π around the core of the vortex, which is a point in $d = 2$ and a line in $d = 3$. Mathematically we can define a vortex as a configuration for which the line integral of $\nabla\theta$ along a closed path $\mathcal{C}$ surrounding the core

$$\oint_{\mathcal{C}} \nabla\theta(\mathbf{r}) \cdot \mathrm{d}\mathbf{l} = 2\pi n, \tag{3.1}$$

where n is the winding number of the vortex. The motivation for such a definition is that we are looking for a stable object which increases entropy at a low cost. Since the angle of the spin changes continuously around a vortex the energy cost is not too large. If we place the vortex depicted in Fig. 3.2 left panel, in the center of the coordinate system and use polar coordinates $\mathbf{r} = \{\rho, \varphi\}$, we get the following expression for the phase of the vortex: $\theta(\mathbf{r}) = \varphi + \pi/2$. We see that $\nabla\theta(\mathbf{r}) = \frac{1}{\rho}\hat{e}_\varphi$, and the total energy of one vortex is

$$E \sim \int_\xi^R (\nabla\theta)^2 \rho \mathrm{d}\rho\mathrm{d}\varphi = 2\pi \int_\xi^R \frac{\mathrm{d}\rho}{\rho} = 2\pi \ln \frac{R}{\xi}, \tag{3.2}$$

where ξ is the radius of the core and R is the size of the system. The logarithmic divergence with respect to system size R means that there is associated an infinite energy cost in inserting a *single* vortex in an infinite system. A pair of vortices of opposite winding however, only affects spins in a limited region around the pair, as

shown the right panel of Fig. 3.2. The energy of such a configuration is finite and this is therefore the relevant excitation in the 2D XY model. In the 3D XY model closed vortex loops are the relevant topological objects.

The vortices of the Ginzburg-Landau model Eq. (2.11) are magnetic flux tubes. They can be either field induced field lines penetrating the sample or thermally induced closed vortex loops. To avoid divergences in $\nabla\theta$, $|\Psi|$ goes to zero inside the core of a vortex. The length scale over which $|\Psi|$ varies is given by ξ in Eq. (2.12), and thus this sets the size of the core. The magnetic field associated with the vortex is shielded over the magnetic penetration depth λ, Eq. (2.12). Since the vortex has a finite range determined by λ, the total energy of a single vortex

$$E \sim \int_{\xi}^{\lambda} (\nabla\theta)^2 \rho \mathrm{d}\rho \mathrm{d}\varphi = 2\pi \int_{\xi}^{\lambda} \frac{\mathrm{d}\rho}{\rho} = 2\pi \ln \frac{\lambda}{\xi}, \tag{3.3}$$

is finite.

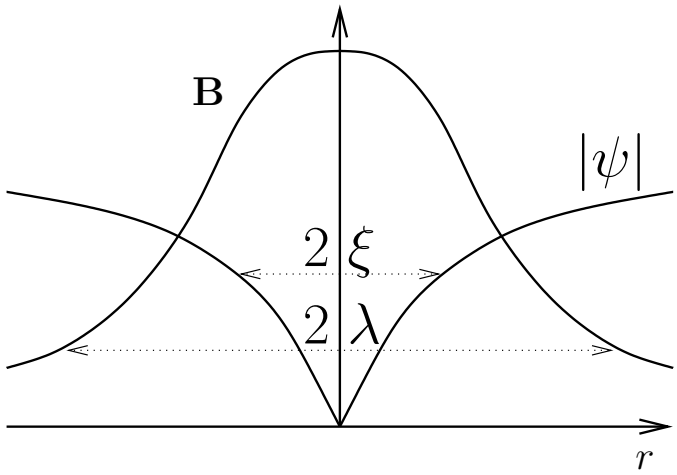

Figure 3.3: Schematic illustration of the size of the core of a vortex determined by ξ, and the range of the vortex determined by λ.

The equation for the supercurrent $\mathbf{J}$ is obtained by varying Eq. (2.11) with respect to $\mathbf{A}$

$$\mathbf{J}(\mathbf{r}) = -\frac{e|\Psi(\mathbf{r})|^2}{m}(\nabla\theta(\mathbf{r}) - e\mathbf{A}(\mathbf{r})). \tag{3.4}$$

Currents flow in a superconductor either close to the surface or close to the center of a vortex. Thus, along a closed contour around a vortex, we have $J = 0$ and hence

$$\oint \mathbf{A} \cdot \mathrm{d}\mathbf{l} = \Phi = \frac{2\pi n}{e}. \tag{3.5}$$

This means that the fluxoid carried by a vortex is quantized to $\Phi_0 = \frac{h}{2e} = 2.067 \cdot 10^{-15}$ Tm^2 (where the Planck constant h has been reinstated).

3.2 Vortex Loop Blowout

In the London approximation $|\Psi|$ is taken to be a constant over the superconductor, and the correlation length is effectively zero. The vortices in this limit are δ-function vortices with zero core size. In zero field the superconductor to normal phase transition is governed by a proliferation of these one dimensional topological objects with quantized flux [40, 50–55]. Snapshots of the proliferation of vortices for the London model taken from a Monte Carlo simulation are shown in Fig. 3.4. For $T < T_c$ there are few vortices indicating a high degree of order and low entropy. At $T = T_c$ the line tension, i.e. the energy cost associated with extending the length of a vortex, goes to zero and all of a sudden there are vortices at all length scales. Consequently the order and the global phase coherence are lost. For even higher temperature the vorticity increases even further.

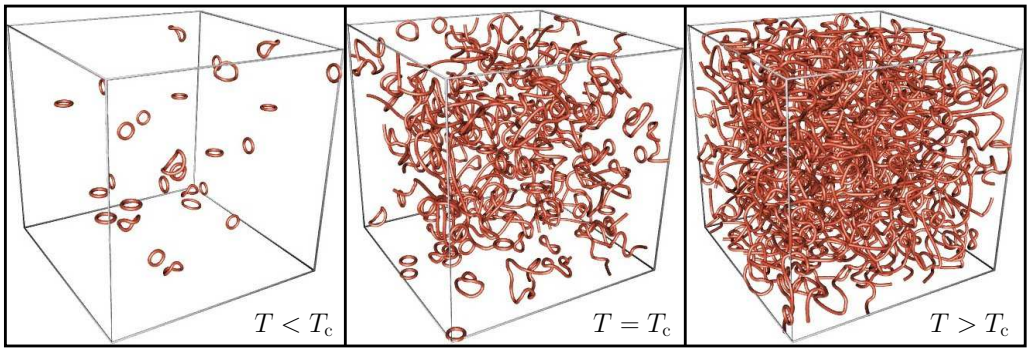

Figure 3.4: Snapshots from a Monte Carlo simulation of the vortex loop blowout in the London model Eq. (2.14) for zero field and $e = 1/\sqrt{2}$. Left panel: $T = 1.25$ ($T < T_c$) deep into the ordered phase there are few vortices and they are of short length. Middle panel: $T = 1.70$ ($T = T_c$) at the transition there are vortices of all lengths and this destroys the order in the system. Right panel: $T = 3.33$ ($T > T_c$) in the disordered phase the system is packed with vortices.

3.3 Vortices of the GL Model in an External Field

The behavior of a type II superconductor exposed to an external magnetic field is quite exotic. This can be seen from the schematic phase diagram given in Fig. 3.5. In the Meissner phase below $B_{c1}(T)$ all magnetic flux tubes are expelled from the superconductor and the system is perfect diamagnetic with zero magnetic field [56]. But above $B_{c1}(T)$ and below $B_{c2}(T)$ some flux lines are allowed into the sample. This phase is called the mixed state or the Abrikosov phase, named after Alexei Abrikosov who in 1957 showed that for $\kappa > 1/\sqrt{2}$ the vortices of the GL model interacted repulsively with each other and that they might form a stable hexagonal lattice [57]. The flux line lattice (FLL) phase between the two solid lines in Fig. 3.5 is characterized by a transverse triangular crystalline order and a finite phase coherence. A rough picture[1] of

[1] The complete story of the behavior of a type II superconductor exposed to a magnetic field is quite involved and still controversial, but this is beyond the scope of this thesis. Some literature on this topic

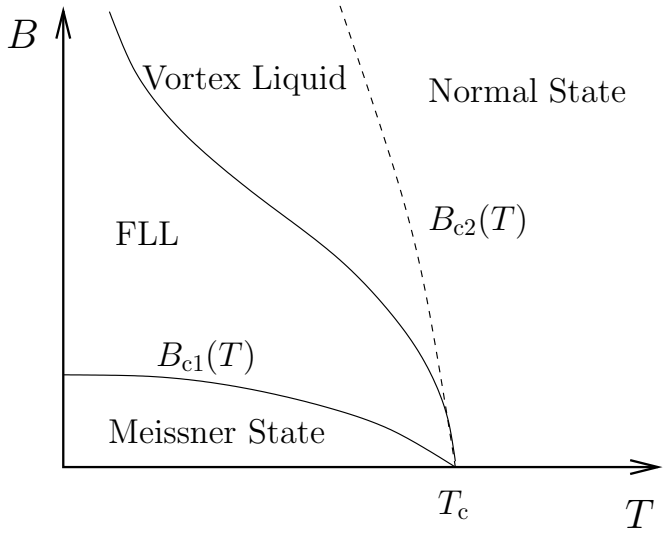

Figure 3.5: Schematic $B-T$ phase diagram for a type II superconductor. The Abrikosov vortex lattice is melted upon crossing the line separating the FLL and the vortex liquid state to destroy superconductivity. The mixed state is between $B_{c1}(T)$ and $B_{c2}(T)$.

what happens to this system upon heating is illustrated by the snapshots of the vortex configurations taken from a Monte Carlo simulation in Fig. 3.6. At low temperature the vortices fluctuate gently around their ground state positions in the FLL. Eventually at $T = T_M$ the thermal fluctuations of the vortices get too strong and the crystalline lattice melts into a vortex liquid phase in which the flux tubes are free to move about. The broken translational symmetry is restored and the transition is a weak first order phase transition [30, 58, 59, 63]. The global phase coherence along with the ability to carry supercurrents in any direction is lost at this point [55, 61]. The line tension of the vortices, however, is finite all the way up to a transition line $T_L(T)$ [54, 55, 61], where it disappears. This line may in fact be thought of as a definition of $B_{c2}(T)$ in the presence of fluctuations, thus elevating it from a cross over line to a true phase transition line (see Fig. 14 of [55]).

3.4 Dualization of the Lattice London Model

A duality transformation can be defined as a mathematical mapping of a theory expressed in one set of variables onto another set of variables. Usually this new set of variables is related to the topological objects of the theory. More rigorously, a duality transformation $\mathcal{D}$ is an operation such that when this is applied to the dual theory H_{dual}

is [54, 55, 58–62].

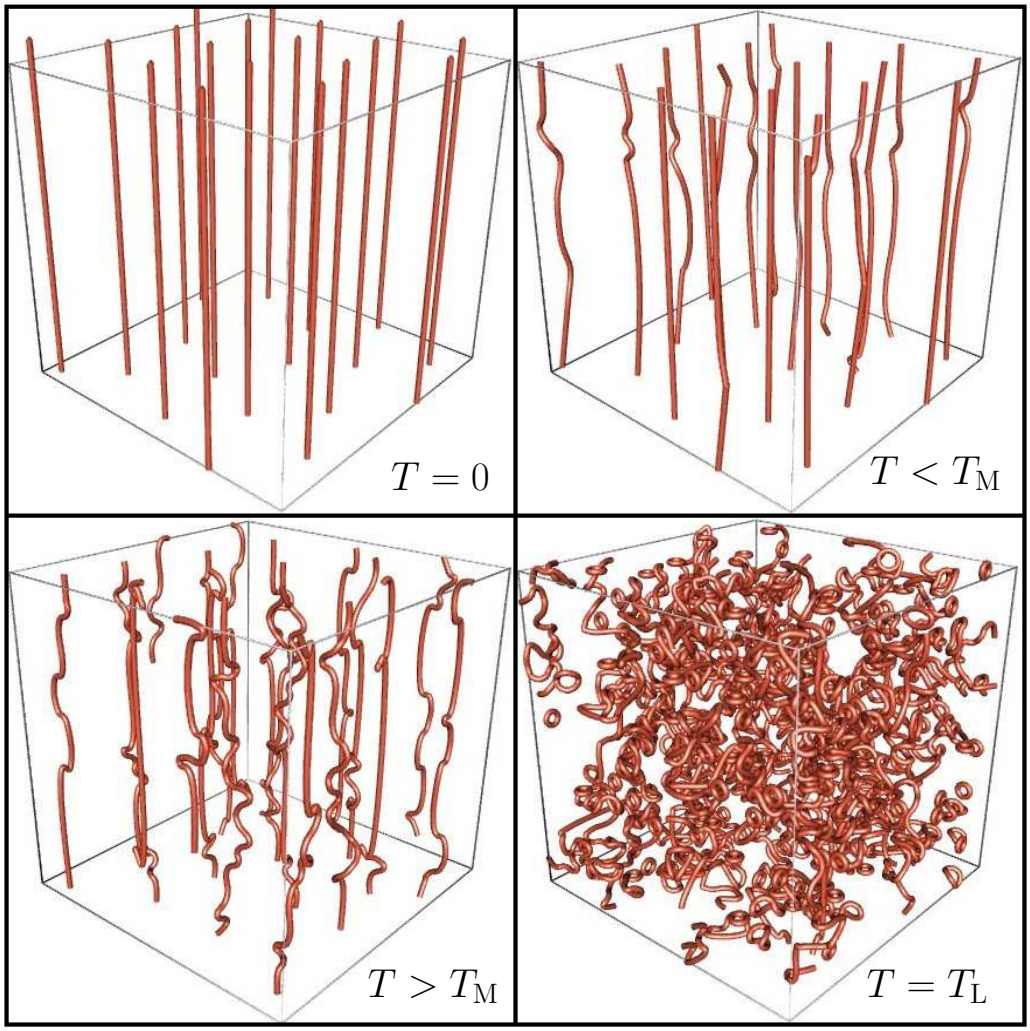

Figure 3.6: Snapshots from a Monte Carlo simulation of the London model Eq. (2.14) for finite field. Upper left panel: $T = 0$ the field induced vortices are arranged in a FLL. Upper right pane: $T = 0.4$ ($T < T_{\mathrm{M}}$) small thermal fluctuations from the FLL. Lower left panel: $T = 0.67$ ($T > T_{\mathrm{M}}$) the thermal fluctuations has melted the FLL and superconductivity is destroyed. Lower right panel: $T = 1.66$ ($T = T_{\mathrm{L}}$) the line tension of the vortices are lost at this temperature.

the original theory H_{org} is recovered;

$$\begin{aligned} \mathcal{D}H_{\mathrm{org}} &= H_{\mathrm{dual}} \\ \mathcal{D}H_{\mathrm{dual}} &= H_{\mathrm{org}}. \end{aligned} \tag{3.6}$$

Unfortunately there is a tendency in the field to denote almost any version of the theory expressed in the topological objects as a dual theory.

Duality in the sense described above was pioneered by Kramers and Wannier in

1941 [64] when they showed how the 2D Ising model can be mapped onto another 2D Ising model. Later on Wegner [65] neatly showed how the technique could be generalized to other models and lattices. Since the new set of variables are the disorder fields, they per definition have small fluctuations when the original variables have large fluctuations and vice versa. Therefore the original and the dual theories have had their high and low coupling regimes interchanged. In the case of Kramers and Wannier their dual theory of the 2D Ising model turned out to be of the same form as the original theory, a so called self-duality. Since the coupling constant of the dual theory is expressed in terms of the original coupling constants, they could easily set them equal to each other and solve for the transition temperature.

There are several reasons for why a duality transformation may be useful. First of all, the dual theory is a description of the topological excitations of the problem, and these constitute the important fluctuations when it comes to destroying the ordered phase. A duality transformation may therefore facilitate a better understanding of the underlying physics of the critical behavior. Second, there might be things that are easier to do with the dual theory than with the original. Perturbation techniques, for instance, are useful in weak coupling regimes, and since the strong and weak coupling regimes are interchanged, other regions of coupling space are accessible for this kind of treatment after a duality transformation.

The following duality transform of the London model Eq. (2.14) is most rigorously done on the lattice, and apart from the Villain approximation it is exact. The Villain approximation is harmless in the sense that it preserves critical properties but renormalizes the coupling constants. Some references to this transformation are [40, 42, 43, 52, 53, 66].

The London model Eq. (2.14) on a 3 dimensional lattice with lattice spacing $a = 1$ is given by the following action and partition function

$$\begin{aligned} \mathcal{Z} &= \int_{-\infty}^{\infty} \mathcal{D}\mathbf{A} \int_{-\pi}^{\pi} \mathcal{D}\theta e^{-S} \\ S_0 &= -\beta \sum_{i\mu} \left[\frac{|\Psi|^2}{2m} \cos(\Delta_\mu \theta_i - eA_{\mu,i}) - \frac{1}{2}(\Delta \times \mathbf{A}_i)_\mu^2 \right], \end{aligned} \tag{3.7}$$

where Δ is the lattice differential operator defined by $\Delta_\mu f(x) = f(x + \hat{e}_\mu a) - f(x)$. First the cosine terms are replaced by a set of quadratic terms with the help of an auxiliary field $\mathbf{n}_i$. This is the Villain approximation [67] which shifts the temperature scale but conserves the critical properties of the model [40],

$$S_1 = \beta \sum_i \left[\frac{|\Psi^2|}{4m} (\Delta\theta_i + 2\pi\mathbf{n}_i - e\mathbf{A}_i)^2 + \frac{1}{2}(\Delta \times \mathbf{A}_i)^2 \right]. \tag{3.8}$$

The next step of the transformation is to perform the Hubbard-Stratonovich decoupling [68, 69], which basically linearizes the coupling between the phase θ_i, the gauge field $\mathbf{A}_i$, and the Villain field $\mathbf{n}_i$ by introducing an auxiliary field $\mathbf{v}_i$ in such a way that when $\mathbf{v}_i$ is integrated out, the original expression is recovered

$$e^{-\frac{\beta|\Psi|^2}{4m}(\Delta\theta_i - e\mathbf{A}_i - 2\pi\mathbf{n}_i)^2} \sim \int_{-\infty}^{\infty} d\mathbf{v}_i e^{-\left[\frac{m}{\beta|\Psi|^2}\mathbf{v}_i^2 - i\mathbf{v}_i(\Delta\theta_i - e\mathbf{A}_i - 2\pi\mathbf{n}_i)\right]}. \tag{3.9}$$

Next a partial summation over the lattice moves the differential operator from θ_i to $\mathbf{v}_i$

$$\sum_i \mathbf{v}_i \cdot \Delta\theta_i = -\sum_i (\Delta \cdot \mathbf{v}_i)\theta_i. \tag{3.10}$$

By neglecting the surface terms this gives the following action

$$S_2 = \sum_i \left[\frac{m}{\beta|\Psi|^2} \mathbf{v}_i \cdot \mathbf{v}_i + \mathrm{i}(\Delta \cdot \mathbf{v}_i)\theta_i + \mathrm{i}2\pi \mathbf{n}_i \cdot \mathbf{v}_i - \mathrm{i}e\mathbf{A}_i \cdot \mathbf{v}_i + \frac{\beta}{2}(\Delta \times \mathbf{A}_i)^2 \right]. \quad (3.11)$$

The Poisson summation formula

$$\sum_{n=-\infty}^{n=\infty} e^{2\pi \mathrm{i} n v} = \sum_{\hat{v}=-\infty}^{\hat{v}=\infty} \delta(\hat{v} - v), \quad (3.12)$$

where $n, \hat{v} \in \mathbb{Z}$ and $v \in \mathbb{R}$, constrains $\mathbf{v}_i$ to take integer values denoted $\hat{\mathbf{v}}_i$. We integrate out θ_i to produce the constraints $\Delta \cdot \hat{\mathbf{v}}_i = 0$. These constraints are automatically enforced by choosing $\hat{\mathbf{v}}_i = \Delta \times \hat{\mathbf{h}}_i$, where $\hat{\mathbf{h}}_i$ is an integer field

$$S_3 = \sum_i \left[\frac{m}{\beta|\Psi|^2} (\Delta \times \hat{\mathbf{h}}_i)^2 - \mathrm{i}e\mathbf{A}_i \cdot (\Delta \times \hat{\mathbf{h}}_i) + \frac{\beta}{2}(\Delta \times \mathbf{A}_i)^2 \right]. \quad (3.13)$$

Again we use the Poisson formula Eq. (3.12) to replace the fields $\hat{\mathbf{h}}$ with a real valued dual field $\mathbf{h}$ at the expense of introducing the term $2\pi\mathrm{i}\mathbf{h} \cdot \mathbf{m}$

$$S_4 = \sum_i \left[\frac{m}{\beta|\Psi|^2} (\Delta \times \mathbf{h}_i)^2 - \mathrm{i}e\mathbf{A}_i \cdot (\Delta \times \mathbf{h}_i) + \frac{\beta}{2}(\Delta \times \mathbf{A}_i)^2 + 2\pi\mathrm{i}\mathbf{h}_i \cdot \mathbf{m}_i \right]. \quad (3.14)$$

The integer field $\mathbf{m}_i$ is nothing but the vortices in the theory. In Eq. (3.13) $\hat{\mathbf{h}}_i$ possesses a gauge symmetry which must be preserved so that Eq. (3.14) is invariant with respect to $\mathbf{h}_i \to \mathbf{h}_i + \Delta\chi_i$. This requires the term $\sum_i 2\pi\mathrm{i}\Delta\chi_i \cdot \mathbf{m}_i$ to be zero, which is fulfilled if $\Delta \cdot \mathbf{m}_i = 0$. *Hence the vortex field $\mathbf{m}_i$ is an integer valued field with zero divergence, i.e. closed loops.*

At this point it is customary to express the theory in the Fourier representation

$$\begin{aligned} S_5 = \sum_{\mathbf{q}} \Bigg[& \frac{m}{\beta|\Psi|^2} (\mathbf{Q}_\mathbf{q} \times \mathbf{h}_\mathbf{q})(\mathbf{Q}_{-\mathbf{q}} \times \mathbf{h}_{-\mathbf{q}}) + \pi\mathrm{i}(\mathbf{h}_\mathbf{q} \cdot \mathbf{m}_{-\mathbf{q}} + \mathbf{h}_{-\mathbf{q}} \cdot \mathbf{m}_\mathbf{q}) \\ & - \frac{\mathrm{i}e}{2} \left[\mathbf{A}_\mathbf{q} \cdot (\mathbf{Q}_{-\mathbf{q}} \times \mathbf{h}_{-\mathbf{q}}) + \mathbf{A}_{-\mathbf{q}} \cdot (\mathbf{Q}_\mathbf{q} \times \mathbf{h}_\mathbf{q}) \right] + \frac{\beta}{2} (\mathbf{Q}_\mathbf{q} \times \mathbf{A}_\mathbf{q}) \cdot (\mathbf{Q}_{-\mathbf{q}} \times \mathbf{A}_{-\mathbf{q}}) \Bigg], \end{aligned} \quad (3.15)$$

where $\mathbf{Q}_\mathbf{q} = e^{\mathrm{i}\mathbf{q}\cdot\hat{\mathbf{e}}} - 1$ is the Fourier representation of the lattice difference operator. The functional integration over $\mathbf{A}_\mathbf{q}$ are plain Gaussian integrals which give

$$S_6 = \sum_{\mathbf{q}} \left[\frac{m}{\beta|\Psi|^2} (\mathbf{Q}_\mathbf{q} \times \mathbf{h}_\mathbf{q})(\mathbf{Q}_{-\mathbf{q}} \times \mathbf{h}_{-\mathbf{q}}) + \pi\mathrm{i}(\mathbf{h}_\mathbf{q} \cdot \mathbf{m}_{-\mathbf{q}} + \mathbf{h}_{-\mathbf{q}} \cdot \mathbf{m}_\mathbf{q}) + \frac{e^2}{2\beta} \mathbf{h}_\mathbf{q} \cdot \mathbf{h}_{-\mathbf{q}} \right]. \quad (3.16)$$

Finally by integrating out $\mathbf{h}_\mathbf{q}$ we obtain a theory of self interacting integer vortex loops defined in the grand canonical ensemble

$$\begin{aligned} \mathcal{Z} &= \sum_{\{\mathbf{m}\}} \delta_{\Delta\cdot\mathbf{m},0}\ \mathrm{e}^{-S_7} \\ S_7 &= 2\pi^2\beta \sum_{\mathbf{r},\mathbf{r}'} \mathbf{m}(\mathbf{r}) V(\mathbf{r} - \mathbf{r}') \mathbf{m}(\mathbf{r}'), \end{aligned} \quad (3.17)$$

where $\delta_{x,y}$ is the Kronecker-delta function, $\mathbf{r}$ and $\mathbf{r}'$ are positions on the dual lattice, and the discrete Fourier transform of the vortex interaction potential $V(\mathbf{r}-\mathbf{r}')$ is given by

$$\widetilde{V}(\mathbf{q}) = \frac{1}{|\mathbf{Q_q}|^2 + m_0^2}, \tag{3.18}$$

where $m_0^2 = e^2|\Psi|^2/2m$ defines the bare mass of the problem. This formulation Eq. (3.17) of the theory has been extensively used in Monte Carlo simulations in **Paper IV**, **Paper V**, **Paper VI**, and **Paper VII**.

The London model expressed in the original variables, Eq. (2.14), has long range interaction mediated by the gauge field $\mathbf{A}$, but its vortices have a finite interaction range determined by the bare mass m_0. However, for systems with $e = 0$ like the 3D XY model or a $|\phi|^4$-theory the interaction in the original variables is local, but the interaction among the vortices has infinite range. To shed more light on this it is instructive to formulate a continuum field theory for the vortices, along the lines pioneered by Thomas *et al.* [43] and Hagen Kleinert [40, 53]. Starting from Eq. (3.16) one may introduce a complex matter field ϕ representing the vortices. This matter field couples minimally to the dual field $\mathbf{h}$

$$H = \int \mathrm{d}\mathbf{r} \left[m^2|\phi|^2 + |\phi|^4 + |(\nabla - \mathrm{i}\mathbf{h})\phi|^2 + \frac{(\nabla \times \mathbf{h})^2}{\beta|\Psi|^2/m} + \frac{e^2}{2\beta}\mathbf{h}^2 \right], \tag{3.19}$$

where a core energy term and a steric repulsion term between the vortices have been added. A renormalization group treatment of the term $(e^2/2\beta)\mathbf{h}^2$ yields

$$\frac{\partial e^2}{\partial \ln\, l} = e^2, \tag{3.20}$$

and hence this term scales up to suppress the dual field $\mathbf{h}$. Thus, the dual theory of the London model is a neutral $|\phi|^4$-theory. On the other hand, the dual theory of a neutral model ($e = 0$) contains no such massive term for $\mathbf{h}$. In this case $\mathbf{h}$ possesses a true gauge symmetry, and the dual theory of an original neutral model is a charged theory [70, 71].

3.5 Gauge Field Correlators

Gauge field correlation functions are useful objects to study when considering the critical properties of gauge theories. The main reason is that they provide non-local gauge invariant order parameters for the theories, which in turn enable reliable determination of critical exponents, including anomalous scaling dimensions.

The gauge field propagator $\mathcal{G}_{\mathbf{A}}(\mathbf{q})$ can be related to $\mathcal{G}_{\mathbf{B}}(\mathbf{q})$, Eq. (2.17) [7, 36]. To express $\mathcal{G}_{\mathbf{B}}(\mathbf{q})$ and $\mathcal{G}_{\mathbf{A}}(\mathbf{q})$ in terms of vortex correlators one adds source terms $J_{\mathbf{q}}$ in Eq. (3.15) which minimally couple to the gauge field (for details, see Appendix C **Paper VII**). Then one performs the Gaussian integrals over $\mathbf{A}$ and $\mathbf{h}$ to obtain $\mathcal{Z}_J$, and finally one differentiates

$$\langle A^{\mu}_{\mathbf{q}} A^{\nu}_{-\mathbf{q}} \rangle = \frac{1}{\mathcal{Z}_J} \left. \frac{\delta^2 \mathcal{Z}_J}{\delta J^{\mu}_{-\mathbf{q}} \delta J^{\nu}_{\mathbf{q}}} \right|_{\mathbf{J}_{-\mathbf{q}} = \mathbf{J}_{\mathbf{q}} = 0}. \tag{3.21}$$

The same thing may be done for $\mathcal{G}_{\mathbf{h}}(\mathbf{q})$ and the results are

$$\mathcal{G}_{\mathbf{A}}(\mathbf{q}) = \frac{2/\beta}{|\mathbf{Q_q}|^2 + m_0^2} \left(1 + \frac{\pi^2 \beta e^2 |\Psi|^4}{2m^2 |\mathbf{Q_q}|^2} \frac{\langle \mathbf{m}_q \cdot \mathbf{m}_{-q} \rangle}{|\mathbf{Q_q}|^2 + m_0^2} \right), \tag{3.22}$$

$$\mathcal{G}_{\mathbf{h}}(\mathbf{q}) = \frac{\beta|\Psi|^2/m}{|\mathbf{Q_q}|^2 + m_0^2} \left(1 - \frac{\pi^2 \beta |\Psi|^2}{m} \frac{\langle \mathbf{m}_q \cdot \mathbf{m}_{-q} \rangle}{|\mathbf{Q_q}|^2 + m_0^2} \right). \tag{3.23}$$

In the Higgs phase the gauge field mass $m_{\mathbf{A}}$ scales according to the Ansatz [36] given by Eq. (2.18) and Eq. (2.19)

$$\mathcal{G}_{\mathbf{A}}(\mathbf{q})^{-1}\frac{2}{\beta} = m_{\mathbf{A}}^2 + C|\mathbf{q}|^{2-\eta_{\mathbf{A}}} + \mathcal{O}(|\mathbf{q}|^{\delta}), \tag{3.24}$$

with a corresponding Ansatz for $m_{\mathbf{h}}$ in the disordered phase

$$\mathcal{G}_{\mathbf{h}}(\mathbf{q})^{-1}\frac{\beta|\Psi|^2}{m} = m_{\mathbf{h}}^2 + C|\mathbf{q}|^{2-\eta_{\mathbf{h}}} + \mathcal{O}(|\mathbf{q}|^{\delta}). \tag{3.25}$$

The masses of $\mathbf{A}$ and $\mathbf{h}$ are therefore defined through the $\mathbf{q} \to 0$ limit of the respective Ansätze

$$\begin{aligned} m_{\mathbf{A}}^2 &\equiv \lim_{\mathbf{q}\to 0}\frac{2}{\beta\mathcal{G}_{\mathbf{A}}(\mathbf{q})}, \\ m_{\mathbf{h}}^2 &\equiv \lim_{\mathbf{q}\to 0}\frac{\beta|\Psi|^2/m}{\mathcal{G}_{\mathbf{h}}(\mathbf{q})}. \end{aligned} \tag{3.26}$$

Thus the gauge field masses can be found by measuring vortex correlators followed by a fit for small $\mathbf{q}$ to their respective Ansätze.

The dual field theory of an original neutral model is a charged theory describing an incompressible vortex tangle [70]. The leading behavior of the vortex correlator $\langle \mathbf{m}_{\mathbf{q}} \cdot \mathbf{m}_{-\mathbf{q}} \rangle$ in this case is [70]

$$\lim_{\mathbf{q}\to 0}\langle \mathbf{m}_{\mathbf{q}} \cdot \mathbf{m}_{-\mathbf{q}} \rangle \sim \begin{cases} [1 - C_2(T)]\mathbf{q}^2 & ; T < T_{\mathrm{c}} \\ \mathbf{q}^2 - C_3(T)|\mathbf{q}|^{2+\eta_{\mathbf{h}}} & ; T = T_{\mathrm{c}} \\ \mathbf{q}^2 + C_4(T)\mathbf{q}^4 & ; T > T_{\mathrm{c}}, \end{cases} \tag{3.27}$$

where $\eta_{\mathbf{h}}$ is the anomalous scaling dimension of the dual gauge field $\mathbf{h}$. For $T < T_{\mathrm{c}}$ the mass of the dual gauge field given by Eq. (3.23) and Eq. (3.26) (with $e = 0$ and $m_0 = 0$) is zero, however for $T > T_{\mathrm{c}}$ the $\mathbf{q}^{-2}$ terms in Eq. (3.23) cancel out exactly and the mass $m_{\mathbf{h}}$ attains an expectation value. The anomalous scaling dimension of the dual gauge field is $\eta_{\mathbf{h}} = 1$ in this case.

For the London model, the effective field theory of the vortices is a neutral theory. The vortex tangle is compressible with a scaling Ansatz for the vortex correlator

$$\lim_{\mathbf{q}\to 0}\langle \mathbf{m}_{\mathbf{q}} \cdot \mathbf{m}_{-\mathbf{q}} \rangle \sim \begin{cases} \mathbf{q}^2 & ; T < T_{\mathrm{c}} \\ |\mathbf{q}|^{2-\eta_{\mathbf{A}}} & ; T = T_{\mathrm{c}} \\ c(T) & ; T > T_{\mathrm{c}}, \end{cases} \tag{3.28}$$

where $c(T)$ is a nonzero constant. Consequently, from Eq. (3.22) and Eq. (3.26) (with $e \neq 0$), as $\langle \mathbf{m}_{\mathbf{q}} \cdot \mathbf{m}_{-\mathbf{q}} \rangle$ changes its asymptotic behavior from $\mathbf{q}^2$ to a constant when the vortex loop proliferation transition occurs at T_{c}, the mass $m_{\mathbf{A}}$ drops from a finite value to zero. Likewise, from Eq. (3.23) and Eq. (3.26) (with $e \neq 0$) it follows that the mass of the dual vector field $m_{\mathbf{h}}$ is finite for all temperatures and has a kink at T_{c} [70]. *This is the Anderson-Higgs phenomenon for this system.* A mean field $\epsilon = 4 - d$ expansion [72], a more thorough one-loop renormalization group investigation of the particular case $d = 3$ [73], as well as investigations of truncated non-perturbative renormalization group flow equations [74, 75] all yield the exact result $\eta_{\mathbf{A}} = 4 - d$,

where d is the dimensionality, for this transition. Recently this result has also been verified numerically [36, 70]. Moreover, in reference [73] for the first time the *physical* consequence of $\eta_{\mathbf{A}} = 1$ for a three dimensional system, was formulated. Namely, the magnetic penetration length λ scales with coherence length

$$\lambda \sim \xi^{\frac{d-2}{2-\eta_{\mathbf{A}}}}. \tag{3.29}$$

For $d = 3$, we thus have $\lambda \sim \xi$ when $\eta_{\mathbf{A}} = 1$ and $\lambda \sim \sqrt{\xi}$ when $\eta_{\mathbf{A}} = 0$.

Thus, the phase transitions in $U(1)$ symmetric models in $d = 3$ with one matter field are governed by the proliferation of vortex loops. Models with local $U(1)$ symmetry are said to have phase transitions belonging to the *inverted* 3D XY (or *inverted* $U(1)$) universality class with anomalous dimension $\eta_{\mathbf{A}} = 1$ and dual anomalous dimension $\eta_{\mathbf{h}} = 0$. Whereas models with a global $U(1)$ symmetry have transitions belonging to the 3D XY universality class with anomalous dimension $\eta_{\mathbf{A}} = 0$ and dual anomalous dimension $\eta_{\mathbf{h}} = 1$. *Moreover, the mechanism which destroys the Meissner effect in type II superconductors is the thermally driven proliferation of vortex loops [54, 55, 70]. The mass of the gauge field* $\mathbf{A}$ *and hence the Meissner phase is destroyed by this proliferation.*

4 Monte Carlo Methods

It was shown in Chapter 2 that phase transitions are characterized by non-analyticities in the partition function, which is an integral over all possible configurations of the system. Exact solutions to such integrals are rare, and in general one must resort to some approximation to extract the wanted information from these systems. The largest and most important class of numerical methods used for this statistical physics problem is the Monte Carlo method. The basic idea of Monte Carlo simulations is that, instead of doing the sum over all configurations, to utilize random numbers to mimic the thermal fluctuations of the system from state to state on the computer and then perform simple measurements just as in a real experiment.

The idea of using random processes to solve problems dates back to at least the 18th century with the "Buffon's needle" experiment, consisting of dropping a needle repeatedly onto a piece of paper with evenly spaced lines to calculate the numerical value of π. Later on, under the name of "statistical sampling", it was used to estimate poorly behaving integrals [76]. The modern method of Monte Carlo was developed at Los Alamos during the end of World War II by Nicolas Metropolis, Stanislaw Ulam, and John von Neumann while working on neutron transport in the hydrogen bomb[1]. These calculations were classified information, however, and never published. The first description of the new method and the use of the name Monte Carlo appeared in 1949 [77].

There are a number of excellent books available on Monte Carlo methods. In writing this chapter, I have used references [76, 78–81]. In section 4.1 I sketch the basic idea of Monte Carlo. In section 4.1.1, I explain the celebrated Metropolis algorithm. In section 4.2, I discuss various post processing techniques that we have used. These include error estimates using the Jackknife method, Ferrenberg-Swendsen multi histogram reweighting, and how to extract critical exponents from finite size scaling.

4.1 Doing Integrals with Monte Carlo

To illustrate the idea behind the Monte Carlo procedure I start by showing how one may approximate a simple integral

$$I = \int_a^b f(x)\mathrm{d}x. \tag{4.1}$$

The traditional way of doing this integral numerically is to divide the area under the curve into rectangles with equal base as illustrated in Fig. 4.1, and then perform the

[1] Enrico Fermi supposedly developed the exact same method 14 years earlier but never published his results [76].

sum

$$I_N = \frac{b-a}{N}\sum_{i=1}^{N} f(x_i) \qquad x_i = a + (i - \frac{1}{2})\frac{b-a}{N}. \tag{4.2}$$

The Monte Carlo approach to this is that, instead of choosing x_i sequentially according to Eq. (4.2), to choose x_i randomly according to $x_i = a + (b-a)\varsigma_i$ where $\varsigma_i \in [0, 1\rangle$ is a random number. As N grows the sum Eq. (4.2) will converge towards I.

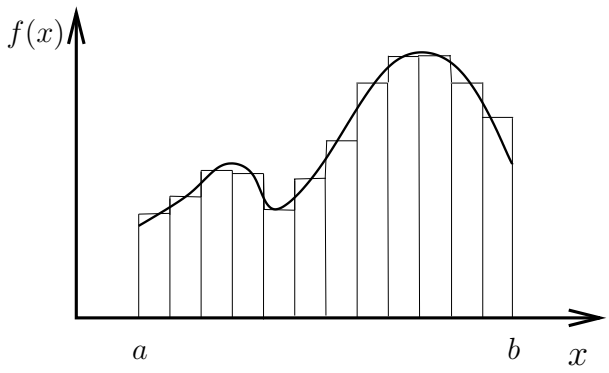

Figure 4.1: The sum of the areas of the rectangles serves as an approximation to the integral I of Eq. (4.1).

In statistical physics we are often interested in integrals of the type

$$\langle O \rangle_f = \int_{-\infty}^{\infty} O(x) f(x) \mathrm{d}x, \tag{4.3}$$

where $O(x)$ is an observable and $f(x)$ is the probability distribution of x. If x_i is chosen randomly according to $f(x)$ we may approximate the integral Eq. (4.3) by the arithmetic mean

$$\overline{O}_N = \frac{1}{N}\sum_{i=1}^{N} O(x_i). \tag{4.4}$$

The standard deviation of the estimator O_N will then be given by

$$\sigma_N^2 = \frac{1}{N}\sum_{i=1}^{N} O^2(x_i) - \left[\frac{1}{N}\sum_{i=1}^{N} O(x_i)\right]^2. \tag{4.5}$$

Now imagine that the important part of $O(x)$ is in a region where $f(x)$ is small and vice versa. The Monte Carlo procedure sketched above will then be inefficient in the sense that much time will be spent on sampling rather unimportant parts of the integral, which again will drive the uncertainty high. One way to circumvent this situation is to introduce a so called importance density $g(x)$ and then redefine the observable

$$\tilde{O}(x) = O(x)\frac{f(x)}{g(x)}. \tag{4.6}$$

The expectation value of the new observable $\tilde{O}(x)$ given by

$$\langle \tilde{O} \rangle_g = \int_{-\infty}^{\infty} \tilde{O}(x) g(x) \mathrm{d}x, \tag{4.7}$$

is the same as $\langle O \rangle_f$. However, the standard deviation of the new observable

$$\tilde{\sigma}_N^2 = \frac{1}{N} \sum_{i=1}^{N} \tilde{O}^2(x_i) - \left[\frac{1}{N} \sum_{i=1}^{N} \tilde{O}(x_i) \right]^2, \tag{4.8}$$

is not the same as σ_N^2. A smart choice of $g(x)$ may therefore reduce the variance dramatically. This concept of reducing the variance is denoted importance sampling. A specific example of this is the Metropolis algorithm.

4.1.1 The Metropolis Algorithm

The statistical physics problem is represented by the evaluation of integrals of the type

$$\langle O \rangle = \frac{\int \mathcal{D}\psi O(\psi) e^{-\beta H[\psi]}}{\int \mathcal{D}\psi e^{-\beta H[\psi]}}, \tag{4.9}$$

where $\mathcal{Z} = \int \mathcal{D}\psi e^{-\beta H[\psi]}$ is the partition function. The number of possible configurations to trace grows exponentially with the system size, thus naive tracing is impossible even for modern day computers. The states ψ are distributed according to the Boltzmann distribution $p_B(\psi) = \mathcal{Z}^{-1} e^{-\beta H[\psi]}$. This is a sharply peaked function, which means that only a few important states account for a dominant part of Eq. (4.9) leaving a huge amount of unimportant states. The strategy is to choose the important states randomly according to p_B by mimicking a physical system with thermal fluctuations. This is done by creating a chain of states where one state evolves stochastically into the other according to some transition rules. Such a chain is called a discrete time Markov chain. The probability of the occurrence of a particular state ψ_i at Markov time n is denoted $p(\psi_i, n)$, and the transition probability from state ψ_i to state ψ_j is denoted $\mathrm{P}(\psi_i \to \psi_j)$. The transition probability $\mathrm{P}(\psi_i \to \psi_j)$ should satisfy the following criteria:

1. $\sum_j \mathrm{P}(\psi_i \to \psi_j) = 1$
2. $\mathrm{P}(\psi_i \to \psi_j)$ should not depend on Markov time n.
3. $\mathrm{P}(\psi_i \to \psi_j)$ should only depend on the properties of the two states ψ_i and ψ_j, not the history of these.

A discrete time Markov chain will fulfill the following master equation

$$p(\psi_i, n+1) = \sum_{j \neq i} \mathrm{P}(\psi_j \to \psi_i) p(\psi_j, n) + [1 - \sum_{j \neq i} \mathrm{P}(\psi_i \to \psi_j)] p(\psi_i, n), \tag{4.10}$$

which basically states that the probability of being in state ψ_i at time $n+1$ is equal to the probability that the system was in state ψ_j at time n and went to ψ_i plus the probability that the system was in state ψ_i and stayed there. Since we want $p(\psi_i, n+1) = p(\psi_i, n) = p_B(\psi_i)$, we get the requirement

$$\sum_i \mathrm{P}(\psi_j \to \psi_i) p(\psi_j) = \sum_i \mathrm{P}(\psi_i \to \psi_j) p(\psi_i). \tag{4.11}$$

The common way to ensure that Eq. (4.11) is fulfilled is to insist on so called detailed balance defined by

$$\mathrm{P}(\psi_j \to \psi_i)p(\psi_j) = \mathrm{P}(\psi_i \to \psi_j)p(\psi_i). \tag{4.12}$$

It is straight forward to show that a Markov chain that fulfills the detailed balance criteria Eq. (4.12), approaches the correct distribution of states $p(\psi_i)$ as n increases [76]. In addition to these requirements the Markov chain should also meet the condition of ergodicity. That is, it should be possible for any state to evolve into any other state in a finite number of Monte Carlo time steps. The obvious reason for this is that according to the Boltzmann distribution any state ψ_i has a finite probability $p_B(\psi_i)$ to occur. If ergodicity is broken and certain states cannot be reached, the Markov chain cannot approach the proper distribution of states.

Rewriting Eq. (4.12) yields

$$\frac{\mathrm{P}(\psi_i \to \psi_j)}{\mathrm{P}(\psi_j \to \psi_i)} = \frac{p(\psi_j)}{p(\psi_i)} = e^{-\beta(H[\psi_j]-H[\psi_i])}, \tag{4.13}$$

thus the transition probabilities can be expressed in terms of the difference in energy in the two states. The original choice by Nick Metropolis [82] was

$$\mathrm{P}(\psi_\mathrm{i} \to \psi_\mathrm{j}) = \min\{1, \mathrm{e}^{-\beta(\mathrm{H}[\psi_\mathrm{j}]-\mathrm{H}[\psi_\mathrm{i}])}\}, \tag{4.14}$$

which along with the algorithm sketched below constitutes the Metropolis algorithm.

1. Start with some initial configuration ψ_i
2. Create a new candidate configuration ψ_j at random
3. Accept the new configuration with probability $\mathrm{P} = \min\left\{1, e^{-\beta(H[\psi_j]-H[\psi_i])}\right\}$
4. Perform measurements
5. Repeat steps 2 - 5 until the results have converged

4.2 Post Processing of Monte Carlo Data

To utilize the output from Monte Carlo simulations efficiently we store time series of various observables such as the energy in files. Afterwards we perform error estimates and reweighting. In this way we do not have to guess equilibration times and autocorrelation times in advance, we merely measure and take care of such things later.

4.2.1 Error Estimates Using Jackknifing

To estimate the accuracy of the Monte Carlo results one traditionally use expressions for the standard deviation such as Eq. (4.5). However Eq. (4.5) is only valid for statistically independent measurements, whereas the Markov chain Monte Carlo procedure produces states that are correlated. Especially around phase transitions temporal correlation is a severe problem. It is possible to account for the correlations [83] by modifying Eq. (4.5) to

$$\sigma_N^2 = \frac{1 + 2\tau/\Delta t}{N-1}\left[\sum_{i=1}^{N} O^2(x_i) - \left(\frac{1}{N}\sum_{i=1}^{N} O(x_i)\right)^2\right], \tag{4.15}$$

where τ is the autocorrelation time and Δt is the time between consecutive measurements. Alternatively one may try to break the dataset down to something which is statistically independent. One such method is the Jackknife method [76, 84, 85].

The idea behind the Jackknife method is to divide the dataset $\{O\}$ of N measurements into J subsets $\{\mathcal{O}_1, \mathcal{O}_2, \ldots, \mathcal{O}_J\}$. If the number of measurements in each subset is larger than the autocorrelation time, the subsets will be statistically independent of each other. Each dataset is then resampled J times by introducing new Jackknife variables and sequentially removing one of the subsets at the time. This may seem like an unnecessary heavy arsenal to pull out just for calculating error bars, but if one is to calculate expectation values and errors of non-linear functions of the observable $f(\langle O \rangle)$, this is one of the few ways to do it. First introduce the Jackknife variable A_i which is the average over all subsets except the one labeled i

$$A_i = \frac{J}{N(J-1)} \sum_{j \notin \mathcal{O}_i} O_j, \tag{4.16}$$

then evaluate the function f in these variables

$$f_i = f(A_i). \tag{4.17}$$

The following Jackknife estimators can then be used to estimate $f(\langle O \rangle)$ and $\sigma^2(f(\langle O \rangle))$

$$\begin{aligned} f_J(\langle O \rangle) &= \frac{1}{J} \sum_i^J f_i \\ \sigma_J^2(f(\langle O \rangle)) &= \frac{J-1}{J} \sum_{i=1}^J \left(f_i - \frac{1}{J} \sum_{k=1}^J f_k \right). \end{aligned} \tag{4.18}$$

4.2.2 Ferrenberg-Swendsen Reweighting

Ferrenberg-Swendsen multi histogram reweighting is a powerful technique that significantly improves the quality of Monte Carlo results. Reweighting takes measurements sampled at one temperature and extrapolates it to other temperatures. The multi histogram method interpolates reweighted results from several Monte Carlo simulations at different temperatures. The idea of reweighting was originally put forward in 1959 [86], but did not catch any attention until Alan Ferrenberg and Robert Swendsen [87] showed how effective the technique could be. The multi histogram technique was then developed shortly afterwards [88, 89]. The reason why it is called histogram reweighting is presumably that at the time Ferrenberg and Swendsen developed these methods disk storage was limited, and instead of storing entire time series of measurements to disk they used histograms. Nowadays disk storage is no major limitation and the reweighting methods are usually implemented without invoking histograms.

Recall the definition of the expectation value of an observable in the notation of statistical physics and how it is sampled in a Monte Carlo simulation

$$\langle O(\beta) \rangle = \frac{1}{\mathcal{Z}(\beta)} \sum_{\{\psi\}} O(\psi) e^{-\beta H[\psi]} = \frac{1}{N} \sum_i O_i, \tag{4.19}$$

the sum over $\{\psi\}$ means trace over all possible states whereas the sum over i runs over all measurements from the Monte Carlo simulation. Now consider the expectation values

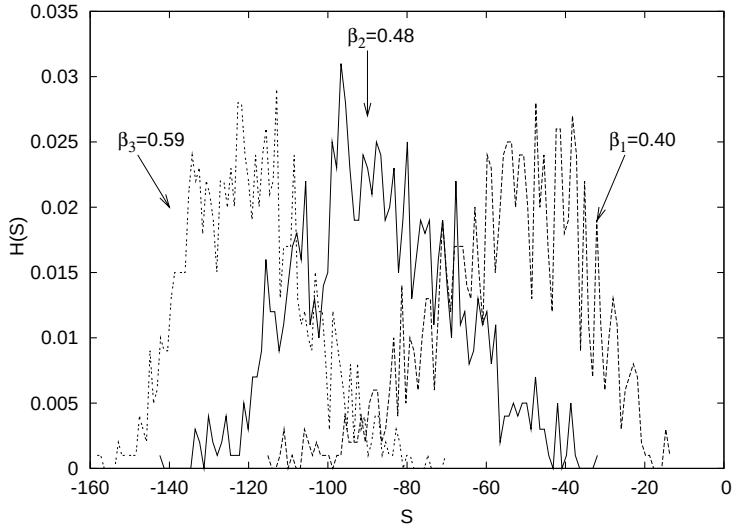

Figure 4.2: Three energy histograms of the 3D XY model for a $4 \times 4 \times 4$ lattice. Reweighting of Monte Carlo data is only reliable between temperatures for which histograms overlap significantly.

of the following observables $Oe^{-(\beta_1-\beta)H}$ and $e^{-(\beta_1-\beta)H}$

$$\begin{aligned} \frac{1}{N}\sum_i O_i e^{-(\beta_1-\beta)H_i} &= \frac{1}{\mathcal{Z}(\beta)}\sum_{\{\psi\}} O(\psi) e^{-(\beta_1-\beta)H[\psi]} e^{-\beta H[\psi]} \\ \frac{1}{N}\sum_i e^{-(\beta_1-\beta)H_i} &= \frac{1}{\mathcal{Z}(\beta)}\sum_{\{\psi\}} e^{-(\beta_1-\beta)H[\psi]} e^{-\beta H[\psi]}. \end{aligned} \tag{4.20}$$

The crucial thing to notice is that the ratio of these two observables are

$$\frac{\sum_i O_i e^{-(\beta_1-\beta)H_i}}{\sum_i e^{-(\beta_1-\beta)H_i}} = \frac{\sum_{\{\psi\}} O(\psi) e^{-\beta_1 H[\psi]}}{\sum_{\{\psi\}} e^{-\beta_1 H[\psi]}}, \tag{4.21}$$

which is precisely the definition of the expectation value $\langle O(\beta_1)\rangle$ at inverse temperature β_1. Thus from a series of measurements $\{O_i\}$ and $\{H_i\}$ collected at one temperature, one may extrapolate the result onto other temperatures by Eq. (4.21). Errors can be estimated exactly the same way as if the results came from a simulation. There is no free lunch however, so this will only work well in a narrow temperature regime. More precisely for reweighting to be reliable from one temperature to another the energy histograms at the two temperatures should overlap significantly. Examples of such histograms for three different coupling constants for the 3D XY model are shown in Fig. 4.2. The histogram for β_2 overlaps with both the histogram for β_1 and for β_3. Thus reweighting of data from β_2 to the range between β_1 and β_2 should work properly. An example of this is shown in Fig. 4.3. The panel to the left shows the specific heat for the 3D XY model with the raw data from the Monte Carlo simulation. In the middle panel the data sampled at $\beta_2 = 0.48$ is reweighted to coupling constants ranging from β_1 to β_3. Note how the error bars increase as the distance over which the data is reweighted increases.

The width of such energy histograms typically decrease with the size of the system, so the larger the system, the smaller range can be successfully reweighted.

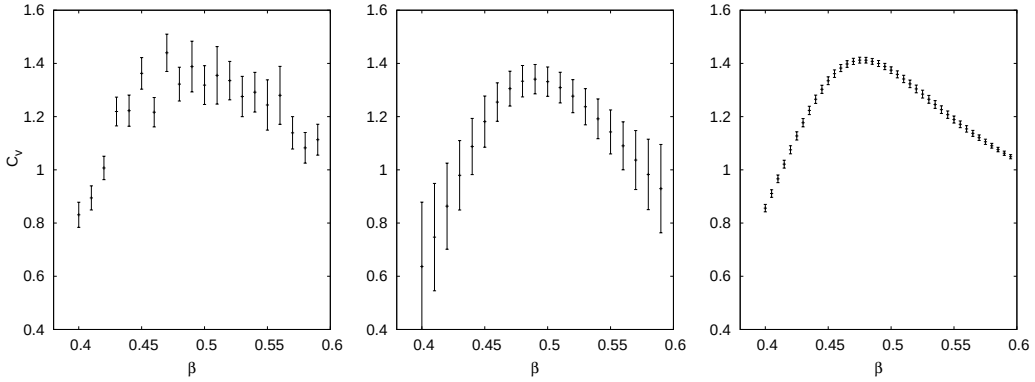

Figure 4.3: The specific heat C_V for the 3D XY model on a $4\times4\times4$ lattice is shown as an example of the output from a Monte Carlo simulation, before and after post processing. The left panel shows C_V calculated directly from the raw data. The middle panel shows an example of plain resampling. The measurements obtained at coupling $\beta_2 = 0.48$ is reweighted to the other values of β. The right panel is an example of full Ferrenberg-Swendsen multi histogram reweighting, for which all of the raw data shown in the left figure is reweighted to all other couplings and then solved self-consistently. Please note the dramatic increase in accuracy after the Ferrenberg-Swendsen reweighting.

The multi histogram method joins together several sets of Monte Carlo data, run at different temperatures, in an optimized way. This relies on estimating the density of states which is a temperature independent quantity. The outline of this is rather involved and for details I refer to the references [76] and [88–90]. Assuming that simulations have been performed on R different couplings β_i with $i \in [1, .., R]$, each consisting of N_i measurements labeled $\alpha_i \in [1, N_i]$. The free energy $F_\beta = -\frac{1}{\beta}\ln \mathcal{Z}(\beta)$ at reweighted temperature β can be expressed in terms of

$$e^{-F_\beta} = \sum_{i=1}^{R}\sum_{\alpha_i=1}^{N_i} \frac{g_i^{-1} e^{-\beta H_i^{\alpha_i}}}{\sum_{j=1}^{R} N_j g_j^{-1} e^{-\beta_j H_i^{\alpha_i} + F_j}}, \tag{4.22}$$

where $g_i = 1 + 2\tau_i$ and τ_i is the autocorrelation time for run number i. Together with the equation $e^{-F_i} = e^{-F_{\beta_i}}$, Eq. (4.22) is solved self-consistently for F_i by some iterative method such as the Newton-Raphson method. The expectation value of an operator O at reweighted temperature is then given by

$$\langle O \rangle_\beta = \sum_{i=1}^{R}\sum_{\alpha_i=1}^{N_i} \frac{O_i^{\alpha_i} g_i^{-1} e^{-\beta H_i^{\alpha_i} - F_\beta}}{\sum_{j=1}^{R} N_j g_j^{-1} e^{-\beta_j H_i^{\alpha_i} + F_j}}. \tag{4.23}$$

The right panel of Fig. 4.3 illustrates the tremendous strength of the multi histogram method. The raw data shown in the left panel is reweighted to the other temperatures and the set defined by Eq. (4.22) is then solved self-consistently. Please note the dramatic enhancement of the data and the decrease in the error bars.

4.2.3 Finite Size Scaling and the Third Moment of the Action

The physics coming out of a computer simulation have size effects just as real experiments. Divergences at phase transitions are smeared out to finite values, discontinuities are rounded, and critical temperatures are shifted. A systematic treatment of these effects can reveal important information of the system. Such an analysis is called finite size scaling (FSS) [17,79], and we have used it extensively to compute critical exponents in all our papers. In particular, we have suggested and benchmarked a new method that utilizes the third moment of the action to extract critical exponents α and ν.

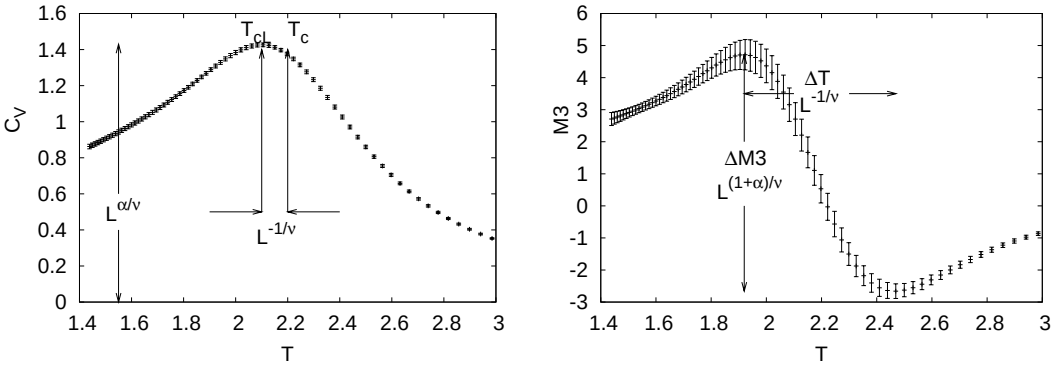

Figure 4.4: The specific heat C_V and the third moment of the action M_3 for the 3D XY model on a $4 \times 4 \times 4$ lattice is shown. The peak to peak value of M_3 denoted ΔM_3 scales with system size according to $L^{(1+\alpha)/\nu}$ and the width between the peaks denoted $\Delta\beta$ scales according to $L^{-1/\nu}$.

Recall from Chapter 2 that the correlation length ζ diverges at the critical point according to $\zeta \sim |T - T_{\rm c}|^{-\nu}$. In a finite system ζ is confined to the size of the system L, so that $\zeta \to L$ as T approaches $T_{\rm c}$, and thus

$$|T - T_{\rm c}| \sim L^{-1/\nu}. \tag{4.24}$$

At the same time the divergence in the specific heat was determined by

$$C_V \propto \frac{\partial^2 F}{\partial T^2} \sim |T - T_{\rm c}|^{-\alpha}, \tag{4.25}$$

and by combining Eq. (4.24) and Eq. (4.25) we get

$$C_V \sim L^{\alpha/\nu}. \tag{4.26}$$

Thus by performing simulations on different system sizes one can in principle extract α and ν, as illustrated in Fig. 4.4, left panel. Scaling relations such as Eq. (4.26) are valid for asymptotically large systems and sufficiently close to the critical point. For small systems there are usually sub-dominant corrections to the leading behavior [17, 91, 92]. This is particularly true for the specific heat for which impractically large systems sizes are needed to bring out the asymptotic behavior [1, 2], see Fig. 4.5.

To get rid of this unwanted analytic background and bring out the leading non-analytic behavior more clearly, we proposed in **Paper I** and **Paper II** [1, 2], to take one

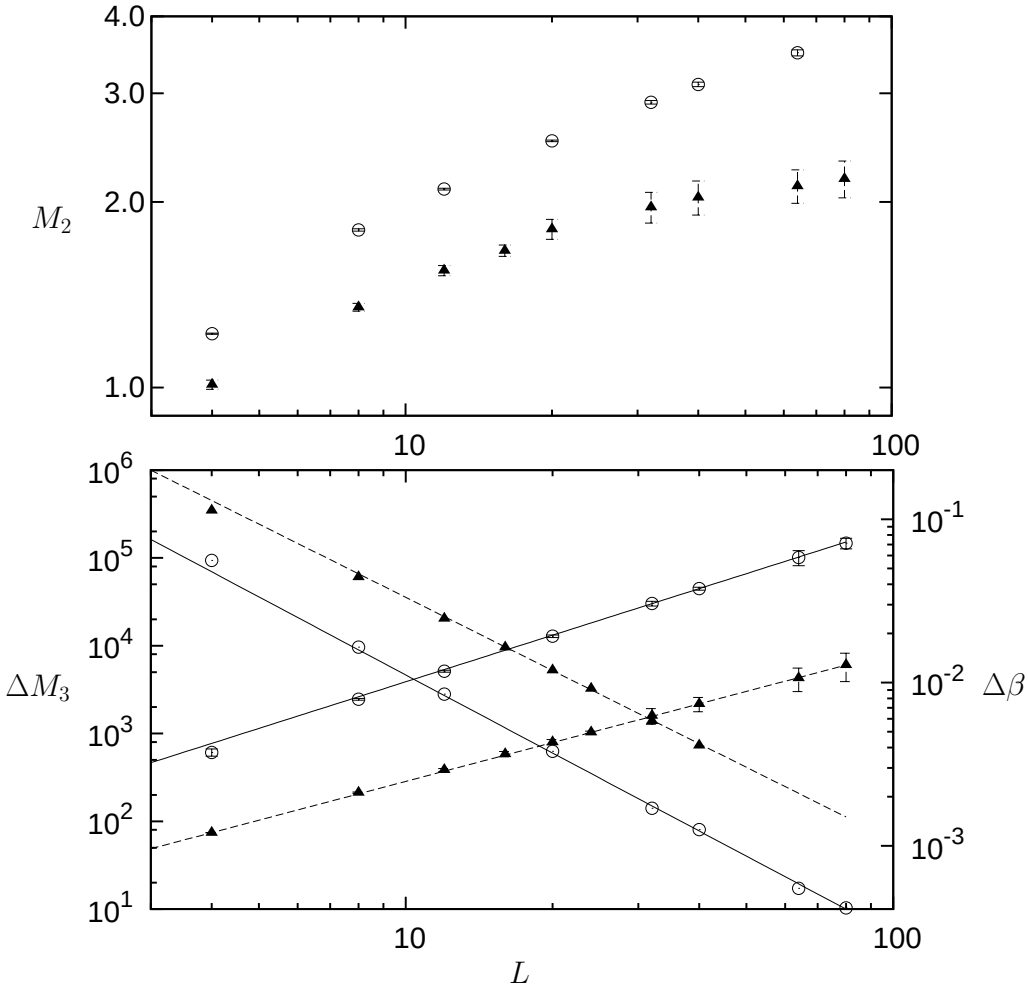

Figure 4.5: FSS plot for the 3D XY (▲) and the 3D Ising model (○). Upper panel: FSS plots of the second moment of the action M_2. Due to large corrections to scaling very large system sizes are necessary to obtain the asymptotic behavior for this quantity. Lower panel: FSS of the peak to peak value ΔM_3 and the width between the peaks $\Delta\beta$ of the third moment of the action M_3. The asymptotic behavior for ΔM_3 and $\Delta\beta$ are achieved for much smaller system sizes than for M_2.

further derivative of the free energy with respect to the temperature

$$\frac{\partial^3 F}{\partial T^3} \sim |T - T_c|^{-(1+\alpha)} \sim L^{(1+\alpha)/\nu}. \tag{4.27}$$

We denote this quantity the third moment of the action M_3, and identify it as the third fluctuation cumulant of the action $S = \beta H$

$$M_3 = \frac{\langle (S - \langle S \rangle)^3 \rangle}{V}. \tag{4.28}$$

Fig. 4.4 right panel shows the scaling properties of M_3. The peak to peak value scales with system size according to $L^{(1+\alpha)/\nu}$ and the width between the peaks scales according to $L^{-1/\nu}$. This provides independent measurements of $(1+\alpha)/\nu$ and $1/\nu$, hence it is possible to calculate both α and ν without invoking the hyperscaling relation Eq. (2.30).

Finite size scaling plots of the second and third moment of the action for the 3D XY and 3D Ising model are given in Fig. 4.5. It is evident that the sub-dominant corrections to scaling are more pronounced for the M_2 scaling plots in the upper panel, than for ΔM_3 and $\Delta\beta$ from the lower panel. Impractically large system sizes are necessary to bring out the asymptotic critical behavior of M_2. Although it is possible to account for the corrections to scaling by invoking a more advanced Ansatz [91]

$$M_2 \sim AL^{\alpha/\nu}\left[1 + BL^{-\Delta/\nu}\right] + K, \tag{4.29}$$

where K originates in the analytic contribution to the free energy and Δ is a correction-to-scaling exponent, this requires more fit parameters and is usually not very successful. The M_3 scaling method on the other hand suffices to bring out the singular part of the free energy more easily. Since the ΔM_3 is defined as the difference between the top and the bottom value of the M_3 curve, see Fig. 4.4, the analytic background term in the Taylor expansion of the scaling function for this quantity cancels altogether. This is the main reason why FSS of the third moment of the action works so well.

Another advantage is that unlike most other successful FSS methods, such as Binder's 4th cumulant method, the M_3 method does not invoke order parameters. Many gauge theories do not have a well defined order parameter, and even in the cases where an order parameter is defined it is usually hard to compute numerically. The third moment of the action is a purely thermodynamic quantity which is always easily accessible from MC simulations.

4.2.4 Lee-Kosterlitz Method

First order transitions are hard to deal with on the computer. As opposed to second order phase transitions these have no diverging length scale and one cannot simply rely on the fact that the physics of the shorter wave lengths are unimportant. Since discontinuities are rounded off by the finite size of the system, it is very problematic to distinguish a weakly first order transition from a second order transition by a purely numerical method. First of all, first order transitions are characterized by the coexistence of the ordered and the disordered phase at the phase transition. In practice this means that some parts of the system are in the ordered state and other parts of the system are in the disordered state. The different parts are separated by some domain surface with dimensionality $d-1$. At the transition there is an equal probability to be in either the ordered or the disordered phase. Lee and Kosterlitz have developed a neat finite size scaling method to determine the order of a transition, based on this idea [93, 94].

They proposed to consider the histogram of the energies $N(E;\beta,L)$ given by

$$N(E;\beta,L) = \mathcal{N}\frac{\rho(E,L)e^{-\beta E}}{\mathcal{Z}(\beta,L)}, \tag{4.30}$$

where $\mathcal{N}$ is the number of Monte Carlo samples, E is the energy of a configuration, L is the system size, $\rho(E,L)$ is the density of states, and $\mathcal{Z}(\beta,L)$ is the partition function. For a first order phase transition the histogram will have a double peak structure, with equal

height for the two coexisting phases. It is clear that $A(E;\beta,L,\mathcal{N}) = -\frac{1}{\beta}\ln N(E;\beta,L)$ is a free energy like quantity which only differs from the Helmholtz free energy F by an additive constant. At the transition

$$A(E_M;\beta,L,\mathcal{N}) - A(E_O;\beta,L,\mathcal{N}) = \Delta F(L) = \frac{1}{\beta}\ln\left(\frac{N(E_O)}{N(E_M)}\right), \tag{4.31}$$

where E_M is the energy of the mixed state, E_O the energy of the pure ordered state, and $\Delta F(L)$ is the free energy barrier separating the two phases. For a first order phase transition this barrier is associated with the tension of the $d-1$ dimensional surface separating the two coexisting phases and this should scale with system size as L^{d-1}. Whereas for a second order transition this barrier should go to zero, i.e. be independent of the system size. Thus to determine the order of a phase transition one should perform finite size scaling of this quantity and if $\Delta F(L) \sim L^{d-1}$ the transition is first order and otherwise if $\Delta F(L) \sim L^0$ the transition is of second order. In **Paper II** we used this method to determine the nature of the transition in the $q = 3$ Abelian Higgs model [2].

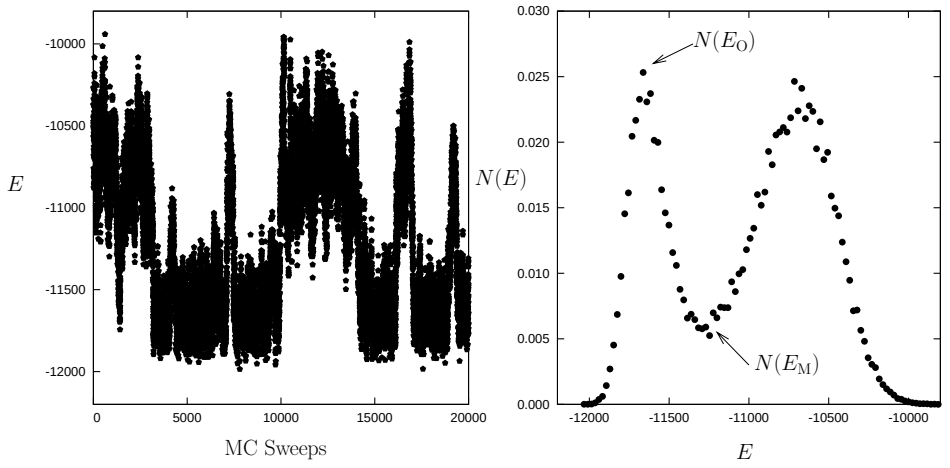

Figure 4.6: Left panel: A time series from a MC simulation of the 3 dimensional Z_3 gauge model [2]. At the transition temperature the system oscillates between the two coexisting phases. Right panel: A histogram of the energy clearly shows the double peak structure which is the hallmark of a first order transition. The free energy like quantity ΔF, defined by Eq. (4.31), can be used to determine the order of the transition by finite size scaling.

5 Liquid Metallic Hydrogen

Hydrogen is the most abundant element in the universe, accounting for about 3/4 of its visual mass. Although atomic hydrogen is the simplest and most understood of the atoms, its condensed states have received remarkably little attention. Condensed hydrogen is projected to have some spectacular features due to its light mass which makes it highly susceptible to quantum effects. In 1935 Eugene Wigner and Hillard Huntington [95] predicted that at a pressure of 25GPa solid molecular hydrogen should dissociate into a monoatomic metal with a bcc structure. Since 1935 the high pressure phases of hydrogen has been projected to exhibit some even more exotic properties. In 1968 Neil Ashcroft predicted that this system would support high temperature superconductivity [96], and in 1974 Brovman, Kagan, and Kholas discussed the possibility of a liquid metallic ground state [97].

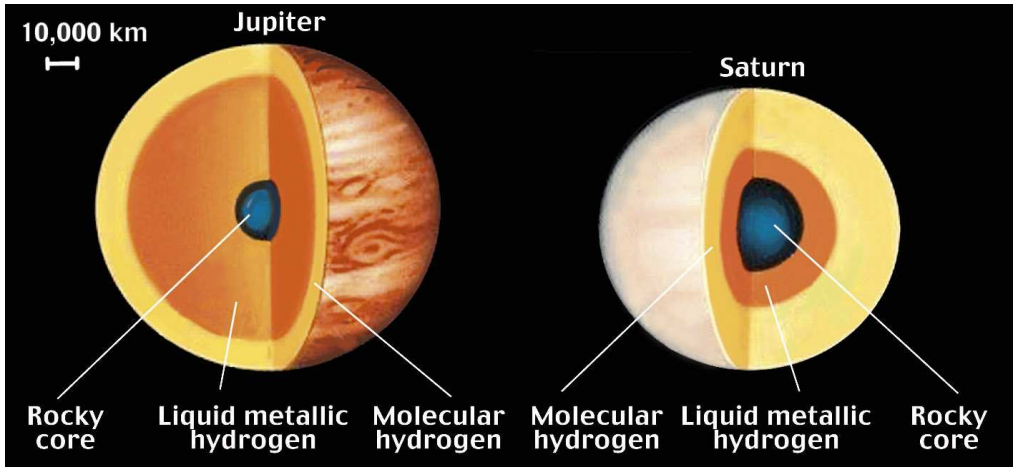

Figure 5.1: The mantles of the giant planets Jupiter and Saturn largely consist of liquid metallic hydrogen. This accounts for their luminosity and large magnetic field. The temperature in the mantles of the planets is too high for superconductivity. Credit: L. Rudnick, University of Minnesota.

At atmospheric pressure molecular hydrogen is an insulator with a band gap of 15eV, but this gap is expected to close at high pressure to produce an insulator to metal phase transition. For high temperatures both the insulating state and the metallic state are liquid. High temperature liquid metallic hydrogen (LMH) is believed to exist in the mantles of the giant planets Jupiter and Saturn as well as in some extrasolar planets.

Jupiter for instance, consists of 90% hydrogen at pressures up to 10TPa, and it is widely accepted that a circulating conducting fluid in the mantle can account for the luminosity and the high magnetic field of the planet [98,99]. Thus the interest in LMH is not merely an academic mind-game, but also a quest to explore the inner structure of the giant gas planets.

The controversy of LMH is related to the projected existence of a liquid metallic ground state [100, 101]. At low temperature and low pressure hydrogen is a molecular solid, and at extreme pressure it is generally assumed that it will form a metallic alkali-like monoatomic crystal [102, 103]. As the density of protons increases with pressure, the zero-point energy increases whereas the ordering energies arising from interactions decrease. In combination with the light mass this has lead to speculations that, like in ^{4}He, there might be a range of densities where hydrogen exhibits a liquid ground state. This liquid metallic state would have to be between the molecular solid and the monoatomic solid phase. A schematic phase diagram for hydrogen is shown in Fig. 5.2.

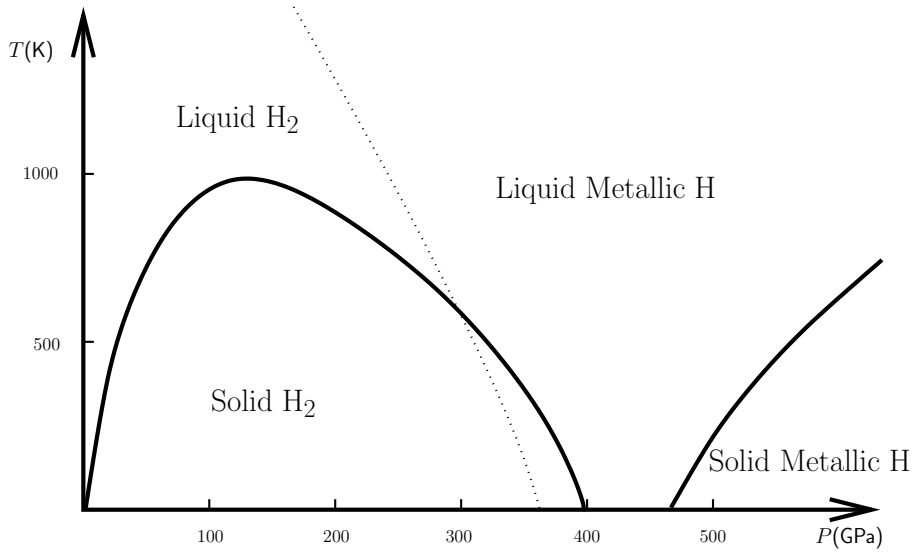

Figure 5.2: A schematic temperature versus pressure phase diagram for hydrogen. The dotted line represents the metal-insulator transition, but only a few points around 140GPa and 3000K confirm this line experimentally. The projected quantum liquid with superconducting phases, including protonic superconductivity, should appear between the solid insulating H_2 phase and the solid metallic H phase. The solid metallic H phase could exhibit electronic superconductivity [96].

The electron charge distribution of the hydrogen molecule in its ground state is shown in Fig. 5.3. As H_2 molecules are packed tighter and tighter under compression, the tails of the charge distributions of the molecules will start to overlap. This transfers charge density from the molecular bond to intermolecular regions. Finally, at the critical

Wigner-Seitz radius $r_s = 1.33$, defined by

$$\frac{1}{\rho_e} = \frac{4\pi}{3} r_s^3 a_0^3, \tag{5.1}$$

where $a_0 = \frac{\hbar^2}{m_e e^2}$ is the Bohr radius and ρ_e is the electron density of the system, the molecular hydrogen is projected to dissociate into a monoatomic state [100, 104–106]. Depending on the exact pressure versus density curve, $r_s = 1.33$ amounts to about 400GPa. Interestingly, hydrogen may become metallic *prior* to the dissociation of the molecules [106, 107]. Thus, as the molecules disintegrate they enter a liquid state consisting of dissociated electrons and protons. Obviously, for LMH to occur at $T = 0$ the melting line of the solid molecular hydrogen, when temperature is plotted versus pressure, would need to have a maximum value and approach zero. This melting line was recently calculated for pressures up to 250GPa by Stanimir Bonev *et al.* in an *ab initio* molecular dynamic simulation [107]. They predict a maximum at about 82GPa and a negative slope for higher pressures. Furthermore, they provide strong evidence that above 300GPa the molecular solid melts into a metallic liquid and that a quantum fluid will appear at about 400GPa.

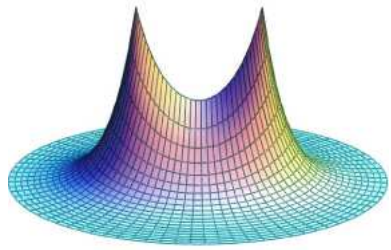

Figure 5.3: The electron charge density of the ground state of a free H_2 molecule. The distance between the two nuclei is $1.4a_0 = 0.74$Å.

Experimental realization of LMH in the laboratory has been pursued along two lines; the solid state at low temperature is investigated with static pressure in diamond anvil cells, while the liquid state at high temperature is investigated with dynamic pressure pulses using shock-wave compression. The shock-wave pulses are able to produce an extreme pressure for a short period of time. Conductivity measurements performed by Weir *et al.* [108] show evidence of metallization at 140GPa and 3000K. More recent experiments that combine the diamond anvil cell and the shock wave compression support these findings [109].

Since pressure is simply force divided by area, enormous pressure can be generated by anvils with a very small tip. A diamond anvil cell is depicted in Fig. 5.4. Hydrogen is squeezed in the small container between the tips of the two diamonds and the pressure is applied mechanically by tightening the anvil and fine tuned by inserting gas into membranes surrounding the diamonds. The pressure in the sample is estimated using the ruby scale. The spectral lines of ruby is directly dependent on pressure, and this dependency is measured up to 80GPa and estimates of it is believed to be valid to about 550GPa [102, 110, 111]. Powdered ruby is stored with the sample and the shift in the spectral line can then be used as a pressure calibrant. The limiting factor to

obtain extreme static pressure in the GPa-range is that diamonds break due to crystal imperfections. Recently a breakthrough in diamond synthesis technique was announced at the Carnegie Institution of Washington [112]. With a new homoepitaxial chemical vapor deposition technique single crystal diamonds can be produced at a rate up to 1mm an hour. This new technique also allows for better control of the shape of the diamonds, which opens up the possibility to custom make diamonds for anvil cells. Hopefully this will increase the range of pressure from todays record of 320GPa to about 1TPa [113,114].

Paul Loubeyre and coworkers used a diamond anvil cell to perform the most successful high pressure experiment so far. In an optical study they reached a pressure of 320GPa at 100K. At 290GPa the hydrogen sample started to gradually change color from transparent yellow to orange to red and finally to turn completely opaque at 320GPa [115]. The closing of the optical band gap is a sure sign that something interesting is going on at these extreme pressures. The melting curve of hydrogen on the other hand has been measured up to 44GPa [116, 117], and the results are in excellent agreement with simulations [107].

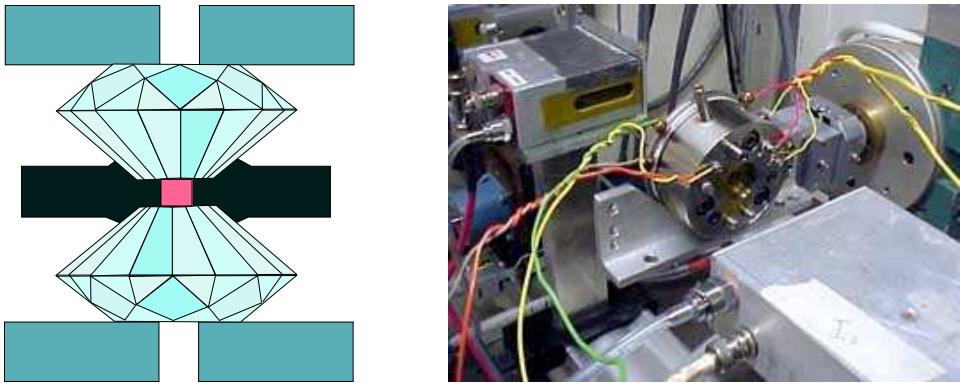

Figure 5.4: A diamond anvil cell is used to compress hydrogen to extreme pressure. Hydrogen is squeezed in the small container between the tips of the two diamonds and the metal gasket. The highest static pressure achieved for hydrogen with this type of experimental setup is 320 GPa, but a promising new homoepitaxial chemical vapor deposition technique will hopefully make it possible to custom make diamonds that can sustain a pressure in the TPa range. Credit: EAS, Cornell University.

5.1 Superconductivity in LMH

According to references [9, 10, 96, 105, 118–120] the quantum liquid consisting of dissociated protons and electrons in LMH should exhibit superconductivity in two channels. At $T_c \sim 100$K electrons should pair up in Cooper pairs [118, 119, 121] and at a significantly lower but finite temperature protons should do the same [9, 10, 100, 120]. The BCS theory predicts that a fermionic system is unstable with respect to perturbations involving pairs of attractive particles at the Fermi sea [122]. The electron electron pairing mechanism in LMH can be explained by invoking a Born-Oppenheimer approximation, by claiming that the dynamics of the protons is slow enough to sustain a sort of electron phonon interaction. The origin of the proton pairing is more controversial however. One

approach is to write down a theory for a general system of electrons and protons with Coulomb interaction. This can be Hubbard-Stratonovich decoupled to give four coupled BCS gap equations. A mean field solution to these equations indeed opens up for attractive interaction between identical particles for wave vectors around to the Fermi sea at finite temperatures [9, 120]. In this case the mechanism is the excitonic interaction. Alternatively, a spin exchange mechanism similar to that of superfluid ^{3}He has also been suggested [101].

Given a system with two superconducting condensates of electrons and protons, one should be able to write down a Ginzburg-Landau functional with two complex scalar wave functions $\Psi^{(1)}(\mathbf{r})$ and $\Psi^{(2)}(\mathbf{r})$, corresponding to protonic and electronic superconducting condensates, respectively. Since the condensates are charged they must be minimally coupled to an electromagnetic gauge field $\mathbf{A}$

$$\begin{aligned} H(\Psi^{(1)},\Psi^{(2)},\mathbf{A}) = \int d\mathbf{r} \Bigg[& \frac{|(\nabla - \mathrm{i}e\mathbf{A})\Psi^{(1)}(\mathbf{r})|^2}{2m^{(1)}} + \frac{|(\nabla - \mathrm{i}e\mathbf{A})\Psi^{(2)}(\mathbf{r})|^2}{2m^{(2)}} \\ & + V(\Psi^{(1)}(\mathbf{r}),\Psi^{(2)}(\mathbf{r})) + \frac{1}{2}(\nabla\times\mathbf{A})^2 \Bigg]. \end{aligned} \tag{5.2}$$

Since Cooper pairs of protons cannot tunnel onto Cooper pairs of electrons and vice versa, there should be no Josephson coupling term in the functional. For this reason the potential term V is a function of $|\Psi^{(1)}|^2$ and $|\Psi^{(2)}|^2$ only. Moreover it is predicted in the literature that this system is a type II superconductor for a certain temperature and pressure range [118,119]. In this case one may consider wave functions of the particular form $\Psi^{(\alpha)}(\mathbf{r}) = |\Psi^{(\alpha)}| \exp\{\mathrm{i}\theta^{(\alpha)}(\mathbf{r})\}$ $\alpha \in \{1,2\}$, thus freezing out amplitude fluctuations in each individual matter field. The potential term V reduces to a constant from which the global values of $|\Psi^{(\alpha)}|^2$ are determined. In fact, for reasons that will become apparent later on, the London approximation will be valid for the low temperature physics of this system no matter if the system is a type I or a type II superconductor. This happens because at low temperature the system is governed by a neutral mode with an infinite penetration depth λ just as for superfluid ^{4}He. Within these assumptions Eq. (5.2) may be rewritten to

$$H = \int d\mathbf{r} \left[\frac{|\Psi^{(1)}|^2}{2m^{(1)}}(\nabla\theta^{(1)} - e\mathbf{A})^2 + \frac{|\Psi^{(2)}|^2}{2m^{(2)}}(\nabla\theta^{(2)} - e\mathbf{A})^2 + \frac{1}{2}(\nabla\times\mathbf{A})^2 \right], \tag{5.3}$$

which is the $N = 2$ component London model[1].

In references [123, 124] it was shown that Eq. (5.3) may be exactly rewritten to the following form

$$\begin{aligned} \mathcal{L} = & \frac{1}{\frac{|\Psi^{(1)}|^2}{2m^{(1)}} + \frac{|\Psi^{(2)}|^2}{2m^{(2)}}} \left[\frac{|\Psi^{(1)}|^2}{2m^{(1)}}\nabla\theta^{(1)} + \frac{|\Psi^{(2)}|^2}{2m^{(2)}}\nabla\theta^{(2)} - e\left(\frac{|\Psi^{(1)}|^2}{2m^{(1)}} + \frac{|\Psi^{(2)}|^2}{2m^{(2)}} \right)\mathbf{A} \right]^2 \\ & + \frac{\frac{|\Psi^{(1)}|^2}{2m^{(1)}}\frac{|\Psi^{(2)}|^2}{2m^{(2)}}}{\frac{|\Psi^{(1)}|^2}{2m^{(1)}} + \frac{|\Psi^{(2)}|^2}{2m^{(2)}}} \left[\nabla\theta^{(1)} - \nabla\theta^{(2)} \right]^2 + \frac{1}{2}(\nabla\times\mathbf{A})^2, \end{aligned} \tag{5.4}$$

where $H = \int d\mathbf{r}\mathcal{L}$. This form of the theory explicitly identifies one charged and one neutral mode. That is, the particular combination $\theta^{(1)} - \theta^{(2)}$ does not couple to the electromagnetic vector potential, i.e. it acts as the theory of superfluid helium, whereas the

[1] The theory Eq. (5.2) is invariant with respect to the transformation $(e \to -e)$ and $(\theta^{(\alpha)} \to -\theta^{(\alpha)})$ for either of the components. Thus it is not necessary to explicitly account for the fact that electrons and protons have opposite charge.

combination $\frac{|\Psi^{(1)}|^2}{2m^{(1)}}\theta^{(1)} + \frac{|\Psi^{(2)}|^2}{2m^{(2)}}\theta^{(2)}$ does couple to the vector potential and behaves like the theory of a superconductor. Physically, the neutral and charged modes correspond to co flows and counter flows of superconducting electrons and protons, respectively.

5.2 Results

In **Paper V**, **Paper VI**, **Paper VII**, and **Paper VIII** this model Eq. (5.3) and its N-component generalization is studied. **Paper V** and **Paper VII** discuss the critical properties of this model in zero magnetic field, whereas **Paper VI**, **Paper VII** and **Paper VIII** discuss the model exposed to an external magnetic field. In this section I give a brief tour of our findings.

By applying the technique described in Chapter 3 (see Appendix B in **Paper VII**), the general N-equivalent of Eq. (5.3) can be rewritten or dualized into a theory of N vortex species $\mathbf{m}^{(\alpha)}$ that interact according to an interaction matrix $D^{(\alpha,\eta)}(\mathbf{r})$ [5, 7]

$$\begin{aligned}\mathcal{Z} = &\sum_{\mathbf{m}^{(1)}} \cdots \sum_{\mathbf{m}^{(N)}} \delta_{\Delta\cdot\mathbf{m}^{(1)},0} \cdots \delta_{\Delta\cdot\mathbf{m}^{(N)},0} \\ &\times \exp\left[-\sum_{\mathbf{r},\mathbf{r}'} \sum_{\alpha,\eta} \mathbf{m}^{(\alpha)}(\mathbf{r}) D^{(\alpha,\eta)}(\mathbf{r}-\mathbf{r}') \mathbf{m}^{(\eta)}(\mathbf{r}') \right],\end{aligned} \tag{5.5}$$

where $\delta_{x,y}$ is the Kronecker delta function. The vortex interaction potential $D^{(\alpha,\eta)}(\mathbf{r})$ is the inverse discrete Fourier transform of

$$\widetilde{D}^{(\alpha,\eta)}(\mathbf{q}) = \frac{\pi^2\beta|\Psi^{(\alpha)}|^2}{m^{(\alpha)}} \left[\frac{\lambda^{(\eta)}}{|\mathbf{Q}_\mathbf{q}|^2 + m_0^2} + \frac{\delta_{\alpha,\eta} - \lambda^{(\eta)}}{|\mathbf{Q}_\mathbf{q}|^2} \right], \tag{5.6}$$

where $\lambda^{(\alpha)} = \frac{|\Psi^{(\alpha)}|^2/2m^{(\alpha)}}{\sum_{\eta=1}^{N} |\Psi^{(\eta)}|^2/2m^{(\eta)}}$, $m_0^2 = e^2 \sum_{\alpha=1}^{N} \frac{|\Psi^{(\alpha)}|^2}{2m^{(\alpha)}}$, and $|\mathbf{Q}_\mathbf{q}|^2$ is the Fourier representation of the lattice Laplace operator. Thus, for $N = 2$ there are two vortex fields that interact with each other through a screened Yukawa potential and an unscreened Coulomb potential. The continuum field theory for this system can be written down along the lines sketched in Chapter 3 by introducing a complex matter field $\phi^{(\alpha)}$ for each vortex species which minimally couples to the dual gauge field $\mathbf{h}^{(\alpha)}$

$$\begin{aligned}H_{\text{dual}} = \int \mathrm{d}\mathbf{r} \Bigg[&\sum_{\alpha=1}^{N} \left(m_\alpha^2 |\phi^{(\alpha)}|^2 + |(\nabla - \mathrm{i}\mathbf{h}^{(\alpha)})\phi^{(\alpha)}|^2 + \frac{(\nabla \times \mathbf{h}^{(\alpha)})^2}{\beta|\Psi^{(\alpha)}|^2/m} \right) \\ &+ \frac{e^2}{2\beta} \left(\sum_{\alpha=1}^{N} \mathbf{h}^{(\alpha)} \right)^2 + \sum_{\alpha,\eta} g^{(\alpha,\eta)} |\phi^{(\alpha)}|^2 |\phi^{(\eta)}|^2 \Bigg].\end{aligned} \tag{5.7}$$

For $N = 1$ the term $(e^2/2\beta)\mathbf{h}^2$ scales up and suppresses the $\mathbf{h}$ field. Thus for $N = 1$ the dual theory of the London model is a neutral $|\phi|^4$-theory and vice versa. Assuming the same to hold for $N = 2$, the sum $\sum_{\alpha=1}^{2} \mathbf{h}^{(\alpha)}$ is suppressed so that $\mathbf{h}^{(1)} = -\mathbf{h}^{(2)}$ and we end up with a gauge theory of two complex matter fields minimally coupled to one gauge field. This was precisely the starting point and so the theory is self-dual for $N = 2$ [5, 7, 13, 14].

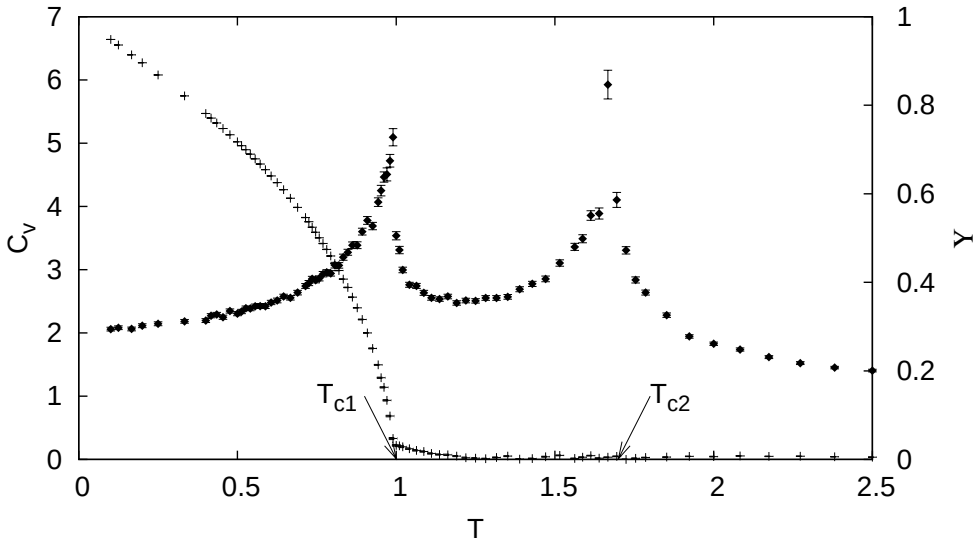

Figure 5.5: MC results of the specific heat C_V (♦) and helicity modulus Υ (+) computed from Eq. (5.3) in zero magnetic field. Two anomalies can be seen in C_V at T_{c1} and T_{c2}, corresponding to a neutral fixed point and a charged Higgs fixed point, respectively. Note how the shape of C_V reveals the nature of the anomalies, at T_{c1} it has the characteristic λ-shape of a 3D XY transition and at T_{c2} it has the characteristic inverted λ-shape of an inverted 3D XY transition. Υ drops to zero as an order parameter at T_{c1}.

5.2.1 Zero Field

In **Paper V** and **Paper VII** we performed MC simulations on this model Eq. (5.5) for $N = 2$ and $|\Psi^{(1)}|^2/2m^{(1)} \neq |\Psi^{(2)}|^2/2m^{(2)}$, the case that is relevant to LMH. The specific heat C_V, shown in Fig. 5.5, exhibits two anomalies at T_{c1} and T_{c2}. FSS analysis of the third moment of the action shows that both anomalies are associated with second order phase transitions with critical exponents α and ν, in agreement with the 3D XY universality class. To determine whether the critical phenomena at T_{c1} and T_{c2} are that of neutral fixed points (3D XY universality class) or of charged fixed points (inverted 3D XY universality class), we used vortex correlators to extract the mass $m_{\mathbf{A}}$ of the gauge field $\mathbf{A}$. Fig. 5.6 clearly shows that the gauge field becomes massive at T_{c2} indicating that this is a charged Higgs fixed point with anomalous scaling dimension $\eta_{\mathbf{A}} = 1$. At T_{c1} $m_{\mathbf{A}}$ is finite but has a kink, thus this is a neutral fixed point associated with the neutral mode in the theory. Since $m_{\mathbf{A}}$ is inversely proportional to the magnetic penetration depth λ, this effect should be directly observable in LMH. To characterize the onset of the neutral mode at T_{c1} further, we calculated the helicity modulus Υ analogous to Eq. (2.10), defined as the second derivative of the low temperature expansion of the free

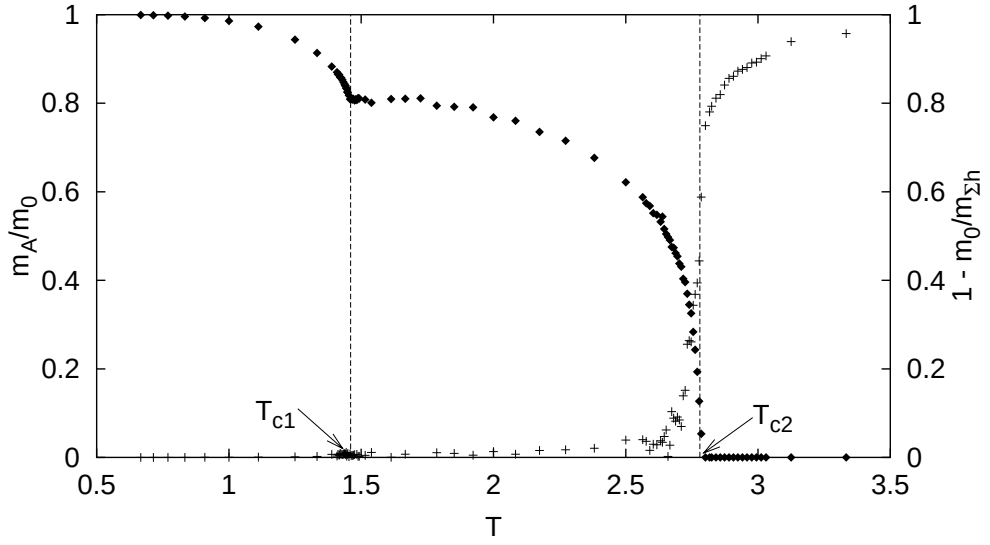

Figure 5.6: MC results of the mass $m_{\mathbf{A}}$ (♦) and $m_{\Sigma\mathbf{h}}$ (+) computed from Eq. (5.5) in zero magnetic field. Two non-analyticities can be seen in $m_{\mathbf{A}}$ at T_{c1} and T_{c2}, corresponding a neutral fixed point and a charged Higgs fixed point, respectively. An abrupt increase in $m_{\Sigma\mathbf{h}}$ due to vortex condensation is located at T_{c2}. Please note that the temperature scale is different from Fig. 5.5 as C_V and Υ are computed from Eq. (5.3) and $m_{\rm A}$ is computed using Eq. (5.5).

energy with respect to a twist in $\theta^{(1)} - \theta^{(2)}$ [8]

$$\begin{aligned}\Upsilon =& \frac{1}{3L^3}\left\langle \sum_{\mathbf{r},\mu} \cos\left(\Delta_\mu(\theta^{(1)}(\mathbf{r}) - \theta^{(2)}(\mathbf{r}))\right)\right\rangle \\ &- \frac{\beta\frac{|\Psi^{(1)}|^2|\Psi^{(2)}|^2}{4m^{(1)}m^{(2)}}}{6L^3(\frac{|\Psi^{(1)}|^2}{2m^{(1)}} + \frac{|\Psi^{(2)}|^2}{2m^{(2)}})}\left\langle \left[\sum_{\mathbf{r},\mu} \sin\left(\Delta_\mu(\theta^{(1)}(\mathbf{r}) - \theta^{(2)}(\mathbf{r}))\right)\right]^2\right\rangle .\end{aligned} \tag{5.8}$$

The results for Υ are given in Fig. 5.5. We see that Υ is finite below T_{c1} and that it drops to zero as an order parameter at the transition. The appearance of the global phase coherence in $\theta^{(1)} - \theta^{(2)}$ at T_{c1}, proves that this point is indeed associated with the spontaneous breaking of the global $U(1)$ symmetry of the neutral mode. Thus the low temperature phase of LMH should sustain both superfluidity and superconductivity. It is quite surprising and highly unexpected that a neutral superfluid mode may arise out of a system consisting of two charged condensates. [11–14]. The

5.2.2 Application to Quantum Antiferromagnets

In **Paper VII** we also investigated the $N = 2$ model with equal phase stiffnesses $|\Psi^{(1)}|^2/2m^{(1)} = |\Psi^{(2)}|^2/2m^{(2)}$. This is the model which is proposed as an effective theory for an easy plane quantum antiferromagnet. The specific heat C_V and the helicity modulus Υ is given in Fig. 5.7, and the mass of the gauge field $m_{\mathbf{A}}$ is given

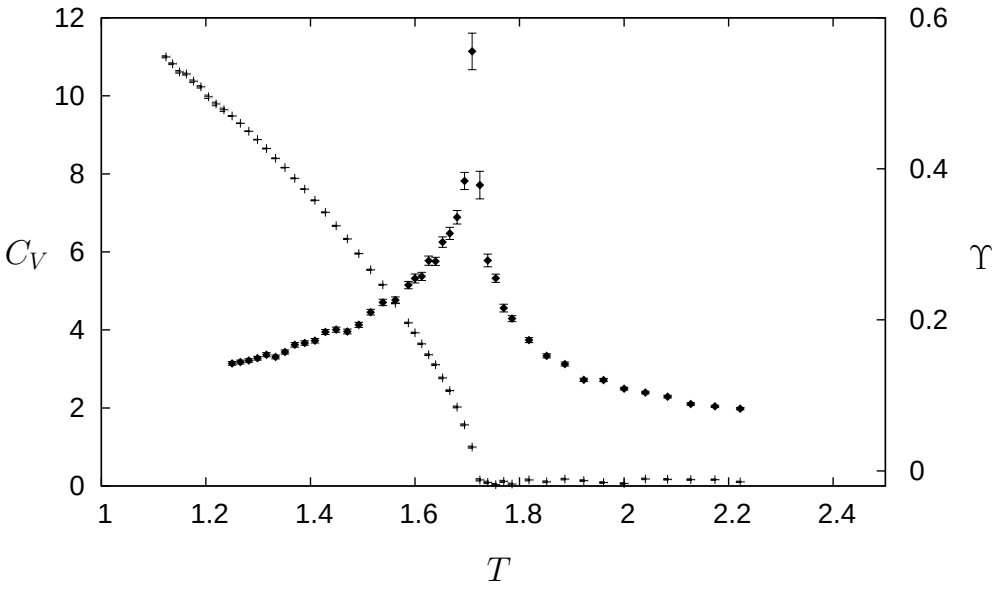

Figure 5.7: MC results of the specific heat C_V (♦) and helicity modulus Υ (+) computed from Eq. (5.3) in zero magnetic field for $|\Psi^{(1)}|^2/2m^{(1)} = |\Psi^{(2)}|^2/2m^{(2)}$. One anomaly can be seen in C_V at T_c. Note that the shape of C_V is more symmetric than the anomalies for $|\Psi^{(1)}| \neq |\Psi^{(2)}|$ in Fig. 5.5, this reflects that this is a self-dual transition. The helicity modulus drops to zero as an order parameter at T_c.

in Fig. 5.8. An important point to notice is that when the two anomalies in C_V for $|\Psi^{(1)}|^2/2m^{(1)} \neq |\Psi^{(2)}|^2/2m^{(2)}$ in Fig. 5.5, one inverted λ and one λ shaped, are collapsed onto one anomaly for $|\Psi^{(1)}|^2/2m^{(1)} = |\Psi^{(2)}|^2/2m^{(2)}$, the result is a symmetric anomaly. One would perhaps have guessed from Eq. (5.3) that since one has two decoupled vortex modes, one neutral mode exhibiting a phase transition in the 3D XY universality class and one charged mode exhibiting a phase transition in the inverted 3D XY universality class, that at $|\Psi^{(1)}|^2/2m^{(1)} = |\Psi^{(2)}|^2/2m^{(2)}$ one would have two such phase transitions superimposed on each other to give a transition in the 3D XY universality class. However, there is a principal distinction from the case when $|\Psi^{(1)}|^2/2m^{(1)} \neq |\Psi^{(2)}|^2/2m^{(2)}$. In the latter case the upper phase transition is always a charged critical point because the neutral mode is not developed. Thus at the upper transition the interaction of vortices is of short range, while at the lower transition there is a proliferation of vortices with long range interaction. However, in the case $|\Psi^{(1)}|^2/2m^{(1)} = |\Psi^{(2)}|^2/2m^{(2)}$, then below the single phase transition *both* vortex modes have neutral vorticity along with charged vorticity and thus this phase transition cannot be mapped onto a superposition of a neutral and a charged fixed point. Also, the fact that the transition is described by self-dual theory invalidates the naive superposition conjecture, since either the 3D XY or the inverted 3D XY phase transitions are self-dual.

The critical exponents for this transition are found to be $\alpha = 0.03 \pm 0.04$ and $\nu =$

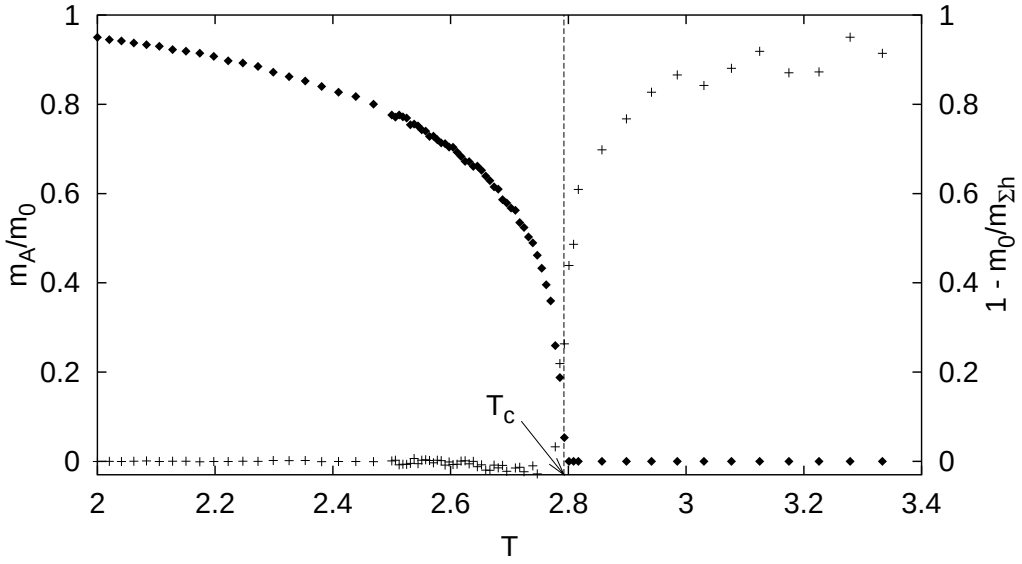

Figure 5.8: The mass of the gauge field $m_{\mathbf{A}}$ (♦) and $1-m_0/m_{\Sigma\mathbf{h}}$ (+) for $|\Psi^{(1)}|^2/2m^{(1)} = |\Psi^{(2)}|^2/2m^{(2)}$. One non-analyticity can be seen in $m_{\mathbf{A}}$ at T_c, corresponding to a fixed point which is not in the 3D XY or inverted 3D XY universality class. An abrupt increase in $m_{\Sigma\mathbf{h}}$ due to vortex condensation is located at $T_c = 2.7(8)$. Please note that the temperature scale is different from Fig. 5.7 as C_V and Υ are computed from Eq. (5.3) and m_A is computed using Eq. (5.5).

0.60 ± 0.02, which is not in agreement with any known universality class. Even though the value of ν appears to be in good agreement with the $3D$ Ising value, we observe that the $3D$ Ising model is not self-dual either, and the new type of critical point for $|\Psi^{(1)}|^2/2m^{(1)} = |\Psi^{(2)}|^2/2m^{(2)}$ can therefore not be in the $3D$ Ising universality class. The origin of the novel exponents is therefore essentially topological, showing that when the vortex loop blowouts of the neutral and charged modes are not well separated, they interact in a non-trivial fashion. Another point worth noticing is that there is an extra symmetry in the problem since one in Eq. (5.3) for $|\Psi^{(1)}|^2/2m^{(1)} = |\Psi^{(2)}|^2/2m^{(2)}$ may interchange the labels of the two condensates. This was pointed out by Senthil *et al.* [11] which argue that the phase transition in this case falls outside the Ginzburg-Landau-Wilson classification scheme, and that it is an example of a new deconfined quantum critical point.

The question of determining the order of the above mentioned phase transition in the degenerate case $|\Psi^{(1)}|^2/2m^{(1)} = |\Psi^{(2)}|^2/2m^{(2)}$ is highly non-trivial. A recent article by Kuklov *et al.* [125] argue that it is a first order transition. We have pursued this further and we have indications that this might be true for some range of coupling constants. To settle this question is extremely numerically demanding and it warrants further investigation.

5.2.3 External Magnetic Field

The exotic phenomena that are encountered when this system is exposed to an external magnetic field are even more spectacular than the one mentioned above. This comes about because the neutral mode should be unaffected by the magnetic field whereas the charged mode should be highly susceptible to the field. Ordinary $N = 1$ type II superconductors subjected to an external magnetic field are known to form a hexagonal Abrikosov lattice of flux lines [57]. This flux line lattice melts in a discontinuous phase transition to destroy superconductivity [59].

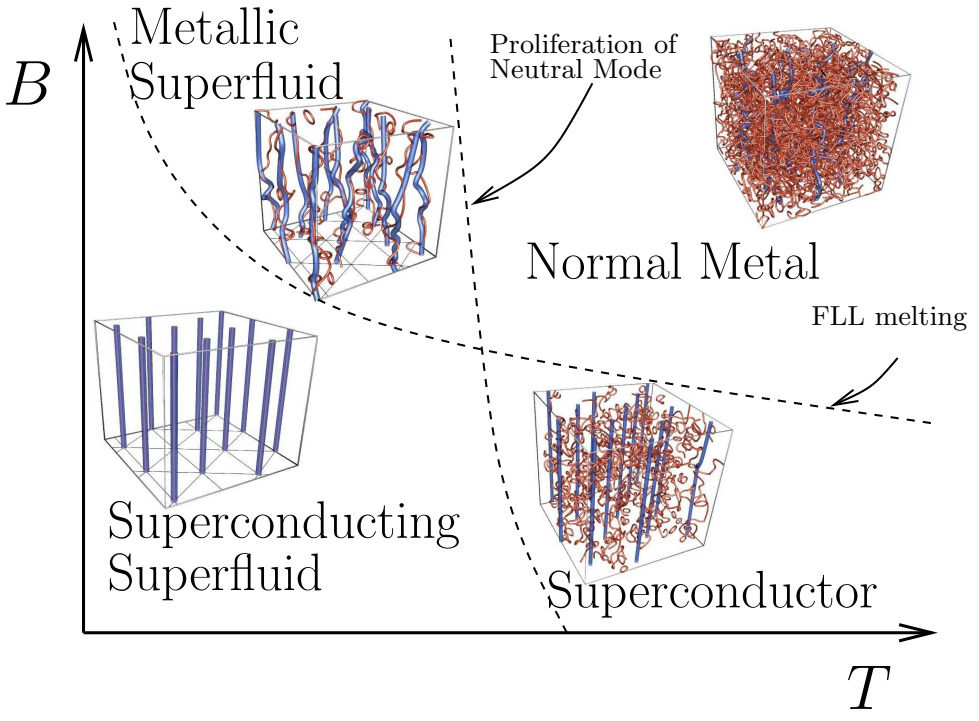

Figure 5.9: The phase diagram of the $N = 2$ model in an external magnetic field contains four phases: a metallic state, an electronic superconducting state, a superfluid superconducting state with both electronic and protonic superconductivity, and a metallic superfluid phases where dissipationless co directed flow of electrons and protons carry no net charge. The latter phase is an entirely novel phase featuring frictionless mass flow and ohmic electronic resistance.

By varying Eq. (5.3) with respect to $\mathbf{A}$ just as in Chapter 3, we obtain the equation for the supercurrent for the system

$$\mathbf{J}(\mathbf{r}) = -\sum_{\alpha=1}^{2}\left[\frac{e|\Psi^{(\alpha)}|^2}{m^{(\alpha)}}\nabla\theta^{(\alpha)}(\mathbf{r}) - e^2\frac{|\Psi^{(\alpha)}|^2}{m^{(\alpha)}}\mathbf{A}(\mathbf{r})\right]. \tag{5.9}$$

If we consider a closed path $\mathcal{C}$ surrounding a single vortex such that only the phase of

the matter field labeled α have a 2π winding

$$\Phi^{(\alpha)} = \oint_{\mathcal{C}} \mathbf{A} \cdot \mathrm{d}\mathbf{l} = \Phi_0 \frac{|\Psi^{(\alpha)}|^2/m^{(\alpha)}}{|\Psi^{(1)}|^2/m^{(1)} + |\Psi^{(2)}|^2/m^{(2)}}, \tag{5.10}$$

we see that a single vortex carries *fractional flux*. The energy of one such field induced individual vortex is logarithmically divergent with respect to the size of the sample. A pair of vortices however, one electronic and one protonic vortex sitting on top of each other, carries integer valued flux. Since the neutral mode $\theta^{(1)} - \theta^{(2)}$ exactly cancels out

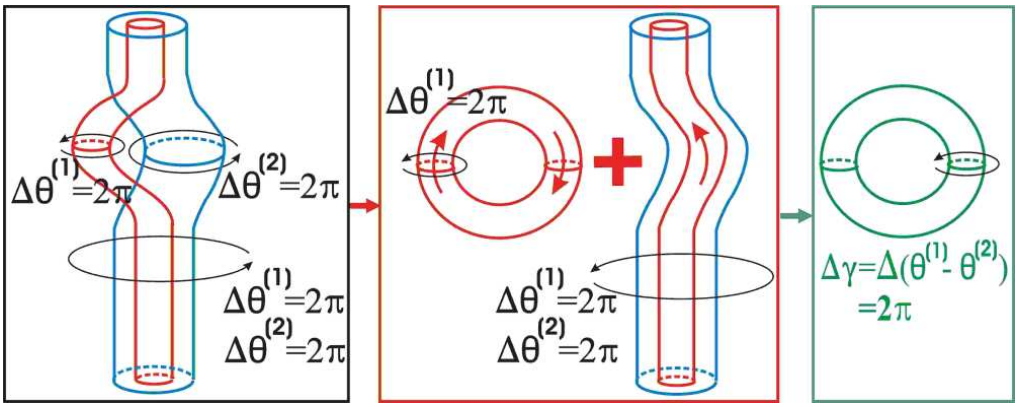

Figure 5.10: Detailed illustration of the low temperature thermal fluctuations in an Abrikosov lattice of composite vortices. A local excursion of the vortex component with lowest bare phase stiffness (protonic vortex) away from the composite vortex lattice may be viewed as a protonic vortex loop superposed on the composite Abrikosov lattice. The composite vortex line does not interact with a vortex with non-trivial winding in $\Delta\gamma = \Delta(\theta^{(1)} - \theta^{(2)})$. A splitting transition of the composite Abrikosov lattice, as is depicted in Fig. 5.12 may thus be viewed as a *zero field* vortex loop proliferation of protonic vortices, with a phase transition in the 3D XY universality class.

for these co centered vortices, they interact with other vortices only through the screened part of the potential Eq. (5.6). For this reason, they have finite energy. Thus the co centered vortices behave just as the vortices of the type II $N = 1$ superconductor, aligning in an Abrikosov lattice in the ground state and melting to destroy superconductivity at some temperature. From the case $N = 1$, the melting temperature of the FLL is known to decrease as the strength of the magnetic field is increased, see Fig. 3.5. The onset temperature of the neutral mode should be unaffected by this. Thus the two lines in the phase diagram, associated with melting of the FLL and the onset of the neutral mode, should cross at some point to span out four different phases [10]. A schematic $B - T$ phase diagram is given in Fig. 5.9.

To track the superconducting properties of this system we probe the lattice ordering of the vortices by computing the planar structure function $S^{(\alpha)}(\mathbf{k}_\perp)$ of the local vorticity $\mathbf{n}^{(\alpha)}(\mathbf{r})$, given by

$$S^{(\alpha)}(\mathbf{k}_\perp) = \frac{1}{(fL^3)^2} \langle |\sum_{\mathbf{r}} n_z^\alpha(\mathbf{r})\ e^{i\mathbf{k}_\perp \cdot \mathbf{r}_\perp}|^2 \rangle, \tag{5.11}$$

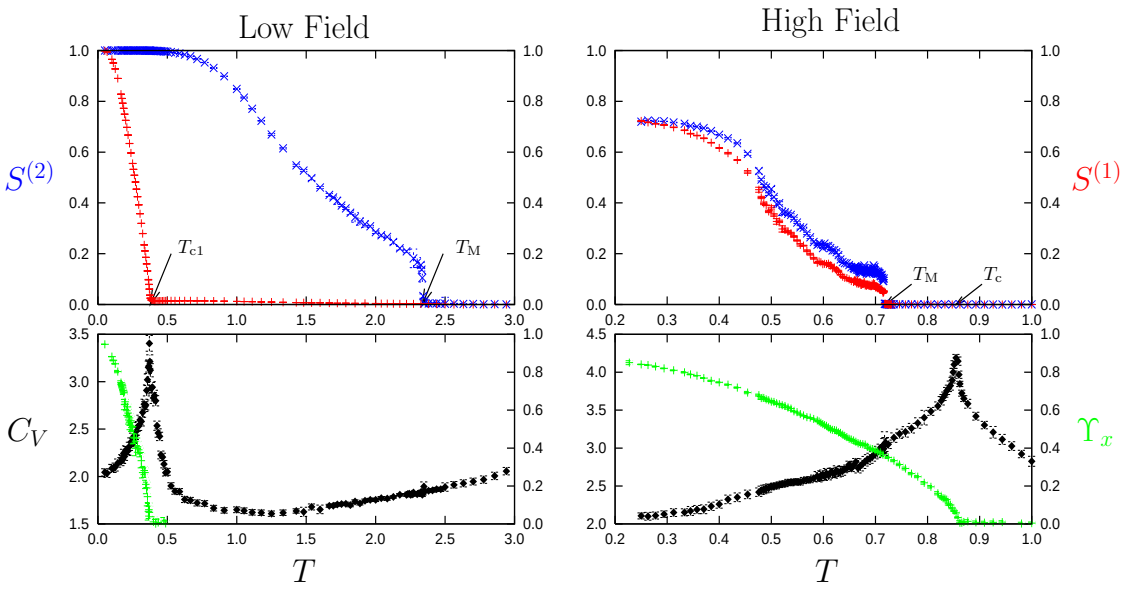

Figure 5.11: Monte Carlo results for the low- (left panel) and high field case (right panel). Low field: the structure factor $S^{(1)}(\mathbf{K})$ (red) for $\mathbf{K} = (\pi/4, -\pi/4)$ drops continuously to zero at T_{c1}. The helicity modulus Υ_x also goes to zero at T_{c1}, and thus both superfluidity and protonic superconductivity are lost. An anomaly in C_V is associated with this transition. At T_M $S^{(1)}(\mathbf{K})$ (red) drops to zero discontinuously. High field: $S^{(1)}(\mathbf{K})$ (red) and $S^{(2)}(\mathbf{K})$ (blue) for $\mathbf{K} = (\pi/4, 2\pi/5)$ drop to zero discontinuously at T_M where the system looses its superconducting properties, but retains superfluidity, as evidenced by a finite helicity modulus Υ_x. At T_c Υ_x drops to zero. C_V has an anomaly associated with this. Note how, in the high field case, there exists a window of temperatures where the structure functions of both the electronic and protonic vortices vanish, while the helicity modulus of the neutral mode remains nonzero. *This is the metallic superfluid.*

where $\mathbf{r}$ runs over sites of the dual lattice and $\mathbf{k}_\perp$ and $\mathbf{r}_\perp$ are perpendicular to $\mathbf{h}$ and f is the magnetic filling fraction. When vortices form a lattice, this function will exhibit a six-fold symmetric Bragg structure, whereas it will feature a characteristic ring structure in the vortex liquid phase. In ordinary $N = 1$ superconductors, the melting of the vortex lattice amounts to a complete destruction of dissipationless currents. To obtain insight into the fate of the superfluid mode of this 2-component system, we measure the ordering in the phase difference $\gamma = \theta^{(1)} - \theta^{(2)}$. The global phase coherence in this variable is probed by the helicity modulus Υ_x, which essentially is the superfluid density, given by Eq. (5.8), in a direction perpendicular to the field.

In the lower part of the phase diagram Fig. 5.9, below the point at which the melting line of the FLL and the line defined by onset of the neutral mode cross, the ground state consists of co centered vortices arranged in an Abrikosov lattice. Snapshots of the vortices are shown in Fig. 5.12 and the MC results are presented in the left panel of Fig. 5.11. Upon increasing the temperature for a fixed magnetic field, the protonic vortices start to tear themselves off the electronic vortices. At T_{c1} there is a critical point where both the

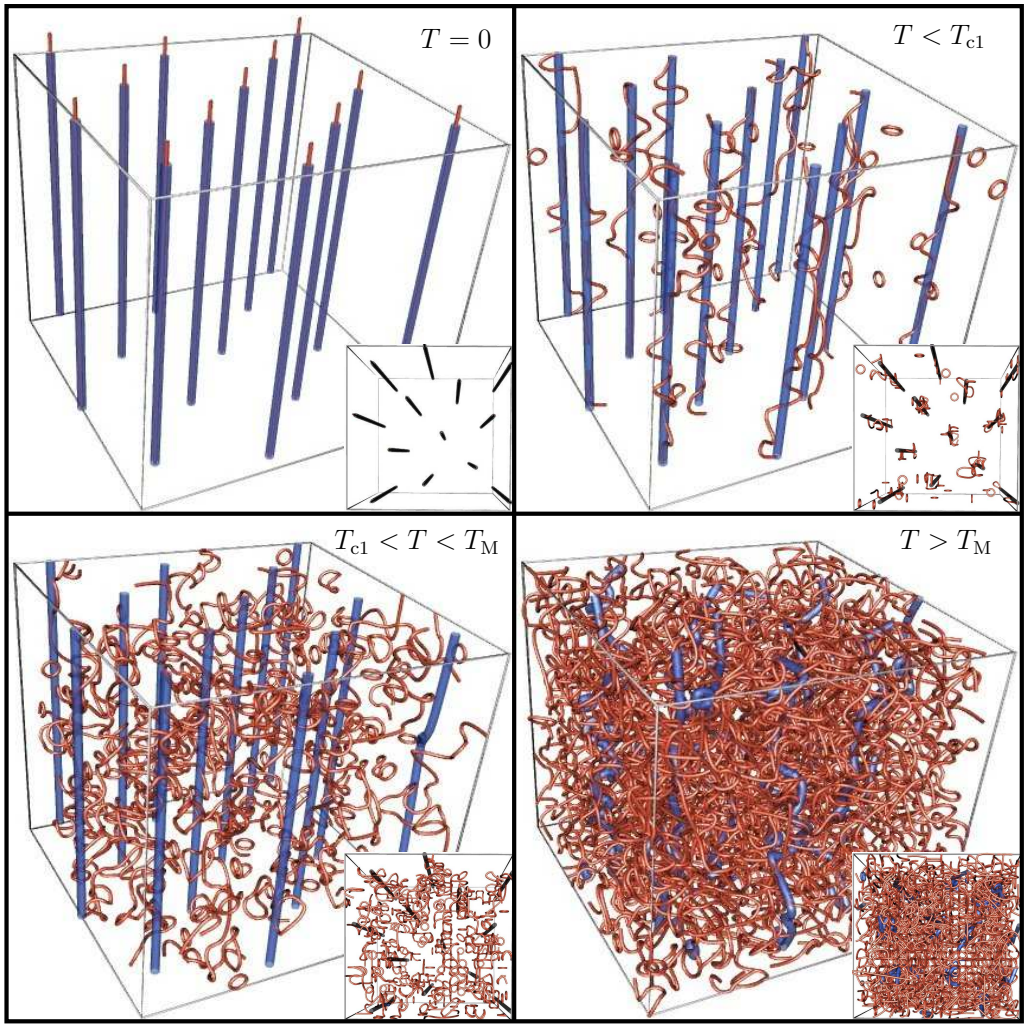

Figure 5.12: Snapshots of the states of vortex matter in the case of low magnetic field generated from MC simulations, taken at four different temperatures: $T = 0$, $T = 0.25$ ($T < T_{c1}$), $T = 0.37$ ($T_{c1} < T < T_M$), and $T = 2.5$ ($T > T_M$). Upper left frame: the ground state consists of electronic (blue) and protonic (red) vortices arranged in a co centered lattice. Upper right frame: for $T < T_{c1}$ protonic vortices only perform small excursions from the lattice. This is the *superconducting superfluid phase*. Lower left frame: for $T_{c1} < T < T_M$ the protonic vortex lattice has melted and the protonic superconductivity is lost, but the electronic vortices are still arranged in a lattice. Lower right frame: for $T > T_M$ the electronic superconductivity is lost.

structure factor $S^{(1)}$ and the helicity modulus Υ_x vanish continuously. The specific heat has an anomaly associated with this temperature and in **Paper VI** we showed that the critical exponents α and ν of this fixed point were those of the 3D XY universality class. The reason for this can be understood by the following physical picture; a small thermal

excursion of a protonic vortex from the FLL can be viewed as a unitary loop of a protonic vortex superimposed on the undistorted FLL, as illustrated in Fig. 5.10. The constituent vortices interact with each other through both a Coulomb and a screened interaction, but with the composite vortices they interact only through the screened interaction. The long distance physics is completely dominated by the Coulomb interaction, and for this reason the process of tearing the protonic (red) vortices off the FLL can be viewed as a proliferation of protonic vortices in zero magnetic field.

In the ground state both the superfluid and the superconducting modes are excited, and the system may be characterized as a superconducting superfluid. At T_{c1} the superfluid property is lost and the system is only able to sustain superconductivity in the electronic condensate. Upon increasing the temperature further, the electronic FLL softens and at $T_{\rm M}$ it melts to destroy the electronic superconductivity. The most remarkable among this series of events is probably the sub-lattice melting of the protonic vortex lattice which happens in a continuous phase transition. Usually melting of mechanical systems are associated with enthalpy and first order transitions, but in this case the broken translational symmetry is not restored until both lattices have melted at $T_{\rm M}$.

For high magnetic field, in the upper part of the phase diagram Fig. 5.9, above the point at which the melting line of the FLL and the line defined by onset of the neutral mode cross, the opposite series of events occur. The MC results are given in the right panel of Fig. 5.11 and snapshots of the different states of vortex matter are given in Fig. 5.13. Upon increasing the temperature from the ground state, both sub-lattices melt at $T_{\rm M}$, and superconductivity in both channels is destroyed. The vortices stay co centered however, and the system is able to sustain superfluidity, as witnessed by the finite Υ_x. This phase is another novel quantum fluid that should be characterized as a superfluid metal. It features frictionless mass flow while at the same time featuring ohmic resistance to flow of charge. At a higher temperature $T_{\rm c}$ the co centered vortices split, Υ_x drops to zero, and the system goes normal.

In conclusion, due to recent advances in diamond synthesis technology, the pressure of 400GPa where hydrogen is projected to become a metallic liquid, appears to be close to realization in diamond anvil cells. If the new state of liquid metallic hydrogen materializes, it should exhibit two novel states that cannot be characterized exclusively as either superconductors or superfluids. The superconducting superfluid state should be able to sustain both co- and counter directed flow of electronic and protonic supercurrents. That is, if the system is exposed to a magnetic field it would set up counter directed supercurrents of electrons and protons at the surface, thus dissipationless transport of charge and mass. On the other hand if the system is rotated it would set up co directed supercurrents of electrons and protons. In this way there will be dissipationless flow of mass, but no net transport of charge. The metallic superfluid state should be able to sustain dissipationless transport of mass in the background of a metallic system. Thus, liquid metallic hydrogen may very well be the next mile-stone within quantum liquids; the next *super state of matter*.

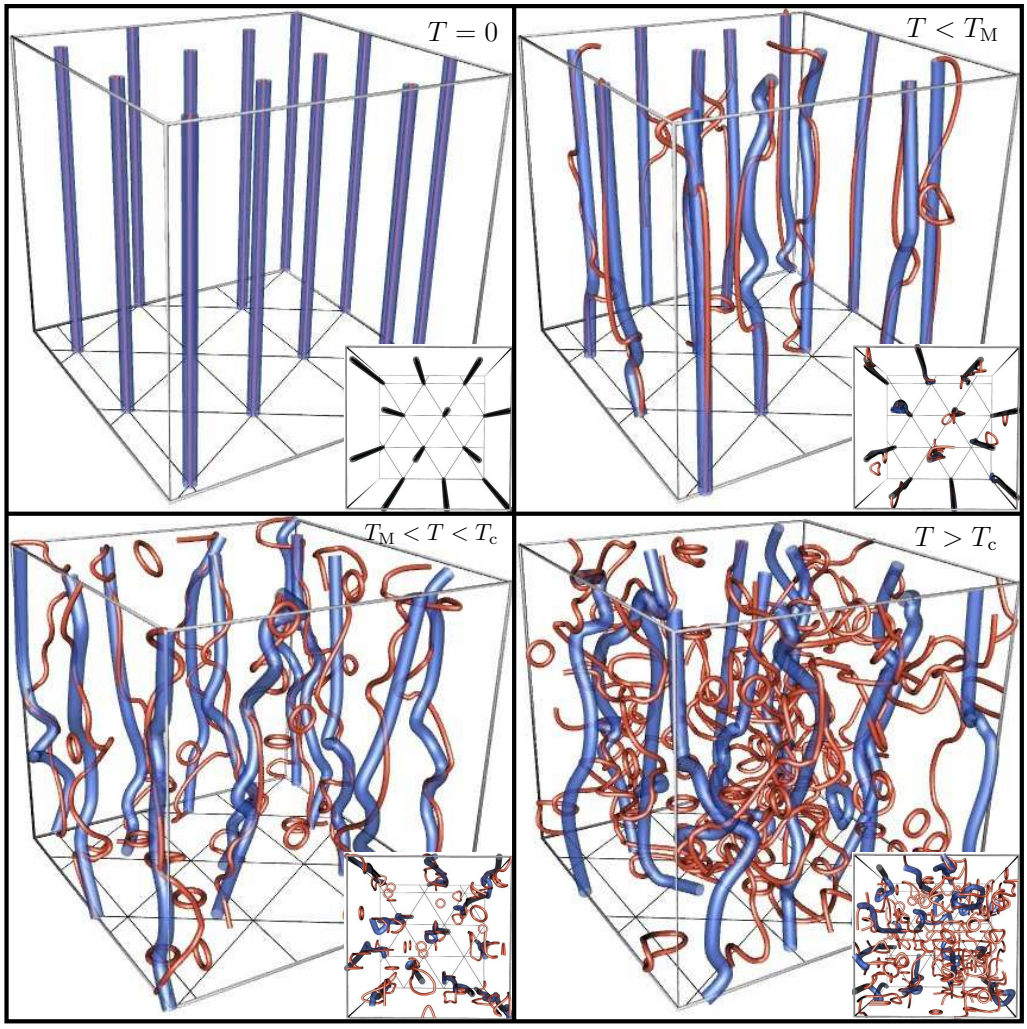

Figure 5.13: Snapshots of the states of vortex matter in the case of high magnetic field generated from MC simulations, taken at four different temperatures: $T = 0$, $T = 0.5$ ($T < T_{\rm M}$), $T = 0.72$ ($T_{\rm M} < T < T_{\rm c}$), and $T = 0.86$ ($T > T_{\rm c}$). Upper left frame: the ground state consists of co centered protonic (red) and electronic (blue) vortices in a FLL. Upper right frame: for $T < T_{\rm M}$ the vortices are arranged in a co centered lattice. Protonic and electronic vortices only perform small excursions from each other. Lower left frame: for $T_{\rm M} < T < T_{\rm c}$ the composite vortex lattice has melted. The electronic and protonic vortices perform stronger excursions from each other, although they essentially remain co centered. *This is the superfluid metallic phase in which co directed currents of protonic and electronic Cooper pairs can propagate dissipationless.* Lower right frame: for $T > T_{\rm c}$ the superfluidity is lost and the electronic and protonic vortices are no longer co centered.

Bibliography

[1] A. Sudbø, E. Smørgrav, J. Smiseth, F. Nogueira, and J. Hove, Phys. Rev. Lett. **89**, 226403 (2002).

[2] J. Smiseth, E. Smørgrav, F. Nogueira, J. Hove, and A. Sudbø, Phys. Rev. B **67**, 205104 (2003).

[3] F. Nogueira, J. Smiseth, E. Smørgrav, and A. Sudbø, Eur. Phys. J. C **33**, 885 (2004).

[4] E. Smørgrav, J. Smiseth, A. Sudbø, and F. S. Nogueira, Europhys. Lett. **68**, 198 (2004).

[5] J. Smiseth, E. Smørgrav, and A. Sudbø, Phys. Rev. Lett. **93**, 077002 (2004).

[6] E. Smørgrav, J. Smiseth, E. Babaev, and A. Sudbø, Phys. Rev. Lett. **94**, 096401 (2005).

[7] J. Smiseth, E. Smørgrav, E. Babaev, and A. Sudbø, Phys. Rev. B **71**, 214509 (2005).

[8] E. Smørgrav, E. Babaev, J. Smiseth, and A. Sudbø, Phys. Rev. Lett **95**, 135301 (2005).

[9] K. Moulopoulos and N. W. Ashcroft, Phys. Rev. Lett. **66**, 2915 (1991).

[10] E. Babaev, A. Sudbø, and N. W. Ashcroft, Nature **431**, 666 (2004).

[11] T. Senthil, A. Vishwanath, L. Balents, S. Sachdev, and M. P. A. Fisher, Science **303**, 1490 (2004).

[12] T. Senthil, L. Balents, S. Sachdev, A. Vishwanath, and M. P. A. Fisher, Phys. Rev. B **70**, 144407 (2004).

[13] O. I. Motrunich and A. Vishwanath, Phys. Rev. B **70**, 075104 (2004).

[14] S. Sachdev, Quantum phases and phase transitions of mott insulators, in *Lecture Notes in Physics: Quantum magnetism*, edited by U. Schollwock, J. Richter, D. J. J. Farnell, and R. A. Bishop, Springer-Verlag, Berlin, 2004.

[15] T. Andrews, Phil. Trans. R. Soc. **159**, 575 (1869).

[16] P. Curie, Ann. Chim. Phys. **5**, 289 (1895).

[17] J. Cardy, *Scaling and Renormalization in Statistical Physics*, Cambridge University Press, Cambridge, 1996.

[18] J. Binney, N. Dowrick, A. J. Fisher, and M. Newman, *The Theory of Critical Phenomena*, Oxforx University Press, Oxford, 1992.

[19] N. Goldenfeld, *Lectures on Phase Transitions and the Renormalization Group*, Addison-Wesley, Reading Massachusetts, 1992.

[20] P. M. Chaikin and T. C. Lubensky, *Principles of condensed matter physics*, Cambridge University Press, Cambridge, 1995.

[21] P. Papon, J. Leblond, and P. H. E. Meijer, *The Physics of Phase Transitions*, Springer-Verlag, Berlin, 2002.

[22] K. G. Wilson, Rev. Mod. Phys. **55**, 583 (1983).

[23] H. E. Stanley, Rev. Mod. Phys. **71**, S358 (1999).

[24] L. Onsager, Phys. Rev. **65**, 117 (1944).

[25] N. D. Mermin and H. Wagner, Phys. Rev. Lett. **17**, 1133 (1966).

[26] V. L. Berezinskii, Sov. Phys. JETP **34**, 610 (1972).

[27] J. M. Kosterlitz and D. J. Thouless, J. Phys. C **6**, 1181 (1973).

[28] M. E. Fisher, M. N. Barber, and D. Jasnow, Phys. Rev. A **8**, 1111 (1973).

[29] Y.-H. Li and S. Teitel, Phys. Rev. B **47**, 359 (1993).

[30] A. K. Nguyen and A. Sudbø, Phys. Rev. B **57**, 3123 (1998).

[31] V. L. Ginzburg and L. D. Landau, Sov. Phys. JETP **20**, 1064 (1950).

[32] S. Elitzur, Phys. Rev. D **12**, 3978 (1975).

[33] P. W. Anderson, Phys. Rev. **130**, 439 (1963).

[34] P. W. Higgs, Phys. Rev. Lett. **13**, 508 (1964).

[35] S. Mo, J. Hove, and A. Sudbø, Phys. Rev. B **65**, 104501 (2002).

[36] K. Kajantie, M. Laine, T. Neuhaus, A. Rajantie, and K. Rummukainen, Nucl. Phys. B **699**, 632 (2004).

[37] B. Widom, J. Chem. Phys. **43**, 3892 (1965).

[38] J. W. Negele and H. Orland, *Quantum Many-Particle Systems*, Addison-Wesley, Redwood City, CA, 1987.

[39] S. Sachdev, *Quantum Phase Transitions*, Cambridge University Press, Cambridge, 1999.

[40] H. Kleinert, *Gauge Fields in Condensed Matter*, World Scientific Publishing, Singapore, 1989.

[41] D. R. Nelson, *Defects and Geometry in Condensed Matter Physics*, Cambridge University Press, Cambridge, 2001.

[42] M. Peskin, Ann. Phys. (N.Y.) **113**, 122 (1978).

[43] P. R. Thomas and M. Stone, Nucl. Phys. B **144**, 513 (1978).

[44] R. Savit, Rev. Mod. Phys. **52**, 453 (1980).

[45] M. B. Einhorn and R. Savit, Phys. Rev. D **19**, 1198 (1979).

[46] M. B. Einhorn and R. Savit, Phys. Rev. D **17**, 2583 (1978).

[47] R. Savit, Phys. Rev. Lett. **39**, 55 (1977).

[48] R. Savit, Phys. Rev. B **17**, 1340 (1978).

[49] J. V. Jose, L. P. Kadanoff, S. Kirkpartick, and D. R. Nelson, Phys. Rev. B **16**, 1217 (1977).

[50] L. Onsager, Nuovo Cimento Suppl. 2 **6**, 249 (1949).

[51] R. R. Feynman, Prog. Low Temp. Phys. **1**, 36 (1955).

[52] C. Dasgupta and B. I. Halperin, Phys. Rev. Lett. **47**, 1556 (1981).

[53] K. Kleinert, Lett. Nuovo Cimento **35**, 405 (1982).

[54] Z. Tešanović, Phys. Rev. B **59**, 6449 (1999).

[55] A. K. Nguyen and A. Sudbø, Phys. Rev. B **60**, 15307 (1999).

[56] M. Tinkham, *Introduction to Superconductivity*, McGraw-Hill, New York, 1996.

[57] A. A. Abrikosov, Sov. Phys. JETP **5**, 1174 (1957).

[58] G. Blatter, M. V. Feigel'man, V. B. Geshkenbein, A. I. Larkin, and V. M. Vinokur, Rev. Mod. Phys. **66**, 1125 (1994).

[59] E. H. Brandt, Rep. Prog. Phys. **58**, 1465 (1995).

[60] Z. Tešanović, Phys. Rev. B **51**, 16204 (1995).

[61] S.-K. Chin, A. K. Nguyen, and A. Sudbø, Phys. Rev. B **59**, 14017 (1999).

[62] K. Fossheim and A. Sudbø, *Superconductivity*, Wiley, London, 2004.

[63] R. E. Hetzel, A. Sudbø, and D. A. Huse, Phys. Rev. Lett. **69**, 518 (1992).

[64] H. Kramers and G. Wannier, Phys. Rev. **60**, 252 (1941).

[65] F. Wegner, J. Math. Phys. **12**, 2259 (1971).

[66] I. F. Herbut, J. Phys. A: Math. Gen. **30**, 423 (1997).

[67] J. Villain, J. Phys. (France) **36**, 581 (1975).

[68] J. Hubbard, Phys. Rev. Lett. **3**, 77 (1959).

[69] R. Stratonovich, Sov. Phys. Dokldy **2**, 416 (1958).

[70] J. Hove and A. Sudbø, Phys. Rev. Lett. **84**, 3426 (2000).

[71] C. de Calan and F. S. Nogueira, Phys. Rev. B **60**, 4255 (1999).

[72] B. I. Halperin, T. C. Lubensky, and S.-K. Ma, Phys. Rev. Lett. **32**, 292 (1974).

[73] I. F. Herbut and Z. Tešanović, Phys. Rev. Lett. **76**, 4588 (1996).

[74] B. Bergerhoff, D. Litim, S. Lola, and C. Wetterich, Int. J. Mod. Phys. A **11**, 4273 (1996).

[75] B. Bergerhoff, F. Freire, D. Litim, S. Lola, and C. Wetterich, Phys. Rev. B **53**, 5734 (1996).

[76] M. E. J. Newman and G. T. Barkema, *Monte Carlo Methods in Statistical Physics*, Oxford University Press, Oxford, 1999.

[77] N. Metropolis and S. Ulam, J. Am. Stat. Assoc. **44**, 335 (1949).

[78] D. P. Landau and K. Binder, *A guide to Monte Carlo Simulations in Statistical Physics*, Cambridge University Press, Cambrigde, 2000.

[79] K. Binder and D. W. Heermann, *Monte Carlo Simulations in Statistical Physics*, Springer-Verlag, Berlin, 2002.

[80] J. M. Thijssen, *Computational Physics*, Cambridge University Press, Cambridge, 1999.

[81] N. Madras, *Lectures on Monte Carlo Methods*, American Mathematical Society, Providence, Rhode Island, 2002.

[82] N. Metropolis, A. W. Rosenbluth, M. N. Rosenbluth, A. H. Teller, and E. Teller, J. Chem. Phys. **21**, 1087 (1953).

[83] P. R. Bevington and D. K. Robinson, *Data Reduction and Error Analysis for the Physical Sciences*, McGraw-Hill, Boston, Ma, 2003.

[84] B. Efron, *The Jackknife, the Bootstrap, and other Resampling Plans*, Society for Industrial and Applied Mathematics, Philadelphia, 1982.

[85] B. Efron, SIAM Review **21**, 460 (1979).

[86] Z. W. Salzburg, J. D. Jackson, W. Fickett, and W. W. Wood, J. Chem. Phys **30**, 60 (1959).

[87] A. M. Ferrenberg and R. H. Swendsen, Phys. Rev. Lett. **61**, 2635 (1988).

[88] A. M. Ferrenberg and R. H. Swendsen, Phys. Rev. Lett. **63**, 1195 (1989).

[89] A. M. Ferrenberg and R. H. Swendsen, Computers in Physics **3(5)**, 101 (1989).

[90] E. P. Münger and M. A. Novotny, Phys. Rev. B **43**, 5773 (1991).

[91] M. Campostrini, M. Hasenbusch, A. Pelissetto, P. Rossi, and E. Vicari, Phys. Rev. B **63**, 214503 (2001).

[92] M. Hasenbusch, K. Pinn, and S. Vinti, Phys. Rev. B **59**, 11471 (1999).

[93] J. Lee and J. M. Kosterlitz, Phys. Rev. Lett. **65**, 137 (1990).

[94] J. Lee and J. M. Kosterlitz, Phys. Rev. B **43**, 3265 (1991).

[95] E. Wigner and H. B. Huntington, J. Chem. Phys. **3**, 764 (1935).

[96] N. W. Ashcroft, Phys. Rev. Lett. **21**, 1748 (1968).

[97] E. G. Brovman, Y. Kagan, and A. Kholas, Sov. Phys. JETP **35**, 783 (1972).

[98] J. J. Fortney, Science **305**, 1414 (2004).

[99] T. Guillot, Phys. Today **57**, 63 (2004).

[100] N. W. Ashcroft, J. Phys.: Condens. Matter **12**, A129 (2000).

[101] N. W. Ashcroft, J. Phys. A: Math. Gen. **36**, 6137 (2003).

[102] H.-K. Mao and R. J. Hemley, Rev. Mod. Phys. **66**, 671 (1994).

[103] N. W. Ashcroft, Condensed matter at higher densities, in *Fenomeni ad alte pressioni, Rendiconti della scula internazionale de fisica "Enrico Fermi"*, edited by R. J. Hemley and G. L. Chiarotti, Societá italiana di fisica, Bologna, 2002.

[104] K. A. Johnson and N. W. Ashcroft, J. Phys.: Condens. Matter **10**, 11135 (1998).

[105] K. A. Johnson and N. W. Ashcroft, Nature **403**, 632 (2000).

[106] R. J. Hemley and N. W. Ashcroft, Physics Today **51**, 26 (1998).

[107] S. A. Bonev, E. Schwegler, T. Ogitsu, and G. Galli, Nature **431**, 669 (2004).

[108] S. T. Weir, A. C. Mitchell, and W. J. Nellis, Phys. Rev. Lett. **76**, 1860 (1996).

[109] P. Loubeyre et al., Int. J. of High Pressure Research **24**, 25 (2004).

[110] J. H. Eggert, K. A. Goettel, and I. F. Silvera, Phys. Rev. B **40**, 5724 (1989).

[111] H.-K. Mao, R. J. Hemley, and M. Hanfland, Phys. Rev. B **45**, 8108 (1992).

[112] R. J. Hemley, Very large diamonds produced, Press Release Carnegie Institution of Washington, May 16, 2005.

[113] R. J. Hemley, Private communication.

[114] C. S. Yan et al., Physica Status Solidi **201**, 24 (2005).

[115] P. Loubeyre, F. Occelli, and R. LeToullec, Nature **416**, 613 (2002).

[116] F. Datchi, P. Loubeyre, and R. LeToullec, Phys. Rev. B **61**, 6535 (2000).

[117] E. Gregoryanz, A. F. Goncharov, K. Matuishi, H.-K. Mao, and R. J. Hemley, Phys. Rev. Lett. **90**, 175701 (2003).

[118] J. E. Jaffe and N. W. Ashcroft, Phys. Rev. B **23**, 6176 (1981).

[119] J. E. Jaffe and N. W. Ashcroft, Phys. Rev. B **27**, 5852 (1983).

[120] K. Moulopoulos and N. W. Ashcroft, Phys. Rev. B **59**, 12309 (1999).

[121] C. F. Richardson and N. W. Ashcroft, Phys. Rev. Lett. **78**, 118 (1997).

[122] J. Bardeen, L. Cooper, and J. R. Schrieffer, Phys. Rev. **108**, 1175 (1957).

[123] E. Babaev, Phys. Rev. Lett. **89**, 067001 (2002).

[124] E. Babaev, L. D. Faddeev, and A. J. Niemi, Phys. Rev. B **65**, 100512 (2002).

[125] A. Kuklov, N. Prokf'ev, and B. Svistunov, cond-mat/0501052 (2005).

Paper I

Criticality in the (2 + 1)-Dimensional Compact Higgs Model and Fractionalized Insulators

Physical Review Letters **89**, 226403 (2002)

Paper II

Phase structure of (2+1)-dimensional compact lattice gauge theories and the transition from Mott insulator to fractionalized insulator

Physical Review B **67**, 205104 (2003)

Paper III

Compact U(1) gauge theories in 2+1 dimensions and the physics of low dimensional insulating materials

European Physical Journal C **33**, 885 (2004)

Paper IV

Phase structure of Abelian Chern-Simons gauge theories

Europhysics Letters **68**, 198 (2004)

Paper V

Critical Properties of the N-Color London Model

Physical Review Letters **93**, 077002 (2004)

Paper VI

Vortex Sublattice Melting in a Two-Component Superconductor

Physical Review Letters **94**, 096401 (2005)

Paper VII

Field- and temperature-induced topological phase transitions in the three-dimensional N-component London superconductor

Physical Review B **71**, 214509 (2005)

Paper VIII

Observation of a Metallic Superfluid in a Numerical Experiment

Physical Review Letters **95**, 135301 (2005)